

# Can Generative Artificial Intelligence Survive Data Contamination? Theoretical Guarantees under Contaminated Recursive Training

Kevin Wang, Hongqian Niu, Didong Li\*

Department of Biostatistics, University of North Carolina at Chapel Hill

## Abstract

Generative Artificial Intelligence (AI), such as large language models (LLMs), has become a transformative force across science, industry, and society. As these systems grow in popularity, web data becomes increasingly interwoven with this AI-generated material and it is increasingly difficult to separate them from naturally generated content. As generative models are updated regularly, later models will inevitably be trained on mixtures of human-generated data and AI-generated data from earlier versions, creating a recursive training process with data contamination. Existing theoretical work has examined only highly simplified settings, where both the real data and the generative model are discrete or Gaussian, where it has been shown that such recursive training leads to model collapse. However, real data distributions are far more complex, and modern generative models are far more flexible than Gaussian and linear mechanisms. To fill this gap, we study recursive training in a general framework with minimal assumptions on the real data distribution and allow the underlying generative model to be a general universal approximator. In this framework, we show that contaminated recursive training still converges, with a convergence rate equal to the minimum of the baseline model's convergence rate and the fraction of real data used in each iteration. To the best of our knowledge, this is the first (positive) theoretical result on recursive training without distributional assumptions on the data. We further extend the analysis to settings where sampling bias is present in data collection and support all theoretical results with empirical studies.

**Keywords:** Generative AI, recursive training, synthetic data, convergence rates

## 1 Introduction

Recent analyses suggest that Artificial Intelligence (AI) generated text, images, and code constitute an increasingly large share of online content. Journalistic investigations have documented widespread use of AI-generated text across platforms such as Wikipedia and

---

\*didongli@unc.edu

hobbyist communities (Froio, 2025), as well as coordinated campaigns on social media (BBC News, 2025). In parallel, empirical research has documented the growing presence of AI-generated content in scientific and academic writing (Brooks et al., 2024; Liang et al., 2024).

Additionally, there has been significant success in training models using synthetic data. Synthetic data has become an important tool in data-scarce settings, for example, through data augmentation in imaging and simulation-based domain randomization (Bowles et al., 2018; Tobin et al., 2017), as well as methods that enable segmentation across modalities without retraining (Billot et al., 2023). Synthetic data is also widely used to enable privacy-preserving data sharing, where a generative model is trained on sensitive data and synthetic samples are released for downstream analysis, as in differentially private generative models and private aggregation of teacher ensembles (Xie et al., 2018; Papernot et al., 2016; Jordon et al., 2018). Beyond data release, synthetic data is increasingly incorporated directly into training pipelines, including data-free knowledge distillation (Lopes et al., 2017; Yin et al., 2020) and self-training methods that learn from model-generated labels (Lee et al.; Xie et al., 2020; Arazo et al., 2020). These widespread applications highlight the practical importance of synthetic data and motivate a theoretical understanding of the behavior of learning systems trained on synthetic datasets.

However, the growing use and prevalence of AI generated synthetic data has raised significant concerns about the long-term behavior of building AI systems trained using both real data generated naturally, as well as synthetic data generated via previous iterations of the AI system. In the real world, practitioners have access to ever increasing amounts of data from the internet, but may not have the ability to reliably distinguish naturally generated samples from synthetic samples. Previous work has theoretically studied the phenomenon of recursive training on purely synthetic data, showing that such models are guaranteed to exhibit “model collapse” in the discrete and Gaussian cases (Shumailov et al., 2023, 2024; Suresh et al., 2024). This work has also empirically suggested that, if purely real data is provided each iteration, then collapse may be avoided. Additionally, Gerstgrasser et al. (2024) provides further empirical evidence that, when the previous training datasets are accumulated over iterations rather than discarded, then the model collapse does appear to be avoided. They also provide theoretical guarantees to explain their experiments, though those theoretical settings are limited to the case of linear models with no new incoming real samples. Thus, the theoretical behavior of contaminated recursive training in the more general setting of generative AI models (i.e., beyond Gaussian and linear) with both real and synthetic data in each iteration remains unknown, leaving an important gap in our knowledge.

In this paper, we fill in this gap by showing, for the first time to the best of our knowledge, that *generative models trained recursively on contaminated data do converge to the desired distribution, without any parametric assumption on the data distribution or the generative model*. However, we show that the resulting convergence rate is determined by the minimum of the convergence rate of the base model and the fraction of real data in each iteration. This shows a phase transition (the baseline convergence rate equals to the fraction of real data) is visualized in Figure 1.

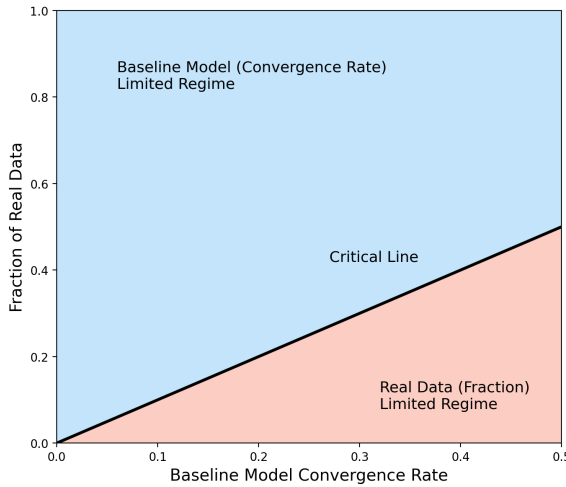


Figure 1: Horizontal axis: convergence rate of the baseline generative model; Vertical axis: the fraction of real data. The color indicates which quantity controls the overall convergence rate: red corresponds to the regime in which the rate is limited by the real-data fraction, blue corresponds to the regime in which the rate is limited by the baseline rate, and the diagonal line marks the phase transition between these two regimes.

In related fashion, generative models trained on biased and non-representative datasets are known to cause significant biases in their generated content (Mehrabi et al., 2021; Zhou et al., 2024). The poor representation or bias in common large datasets used in AI training has been well documented, as well as the downstream effects on popular LLM models such as GPT (Lucy and Bamman, 2021; Sheng et al., 2019). The dangers of this are profound, as content generated by these models can further perpetuate the biases they were trained on, leading to unfair and unjust decisions in critical areas such as justice, welfare, and employment (Mehrabi et al., 2021). Thus an extensive line of work has examined the consequences of training on biased datasets (Zhou et al., 2024; Cross et al., 2024). Although numerous methods have been investigated to mitigate sampling bias (He and Garcia, 2009; Cortes and Mohri, 2014; Chen et al., 2023b), a fundamental question remains unresolved: if a generative model is trained on a biased dataset, how effective are subsequent improved sampling strategies or bias correction methods, in guiding the model toward the true distribution of interest?

To answer this question, we extend our analysis to the recursive contaminated setting where the real data is drawn from biased sampling distributions. We derive conditions under which the generator will either converge to the biased distribution and fail to remove the bias, converge to the true distribution at a slower rate, or converge to the true distribution at the same rate as in the unbiased setting. In particular, if the bias in the real data is not corrected, the generator simply learns the biased distribution and does not recover the true one. If the practitioner reduces bias so that the real sampling distribution converges to

the true distribution fast enough, then the generator converges at the standard rate. If the bias decays too slowly, the generator’s convergence rate is instead limited by the bias’ decay rate. This shows that even when the initial samples are biased, successive improvements in sampling procedure or other bias-correction methods can still lead later iterations of the model to converge.

Taken together, these results show that, under appropriate baseline convergence rate, real data fractions, and bias decay, the generators produced by these recursive procedures can still converge to the true distribution within our framework, even when trained on a mixture of synthetic and potentially biased real data. We support these theoretical results by empirical studies. All proofs and additional experimental details are provided in the Appendix.

## 2 Previous Work

In this section, we review recursive training paradigms that have been studied in the existing literature. Thus far, much of the literature has aimed to study conditions for model collapse under different data contamination schemes in varying recursive training settings. For instance, Shumailov et al. (2024) study iterative training in which each generation is trained *exclusively* on synthetic samples produced by the previous generator. Under discrete and Gaussian models trained by maximum likelihood, they prove that such synthetic-only recursive training inevitably leads to model collapse, and their experiments confirm severe degradation.

Building on this line of work, Suresh et al. (2024) provide explicit collapse rate guarantees for maximum-likelihood training under discrete and Gaussian models, giving quantitative bounds on how quickly recursive training diverges from the target distribution. Again in this setting, the generator for each iteration is trained *exclusively* on synthetic output of the previous iteration’s generator, with no data accumulation across iterations and no re-introduction of real data.

Other works have expanded the synthetic-only data case, and have studied the role of the introduction of real data in recursive training frameworks. Shumailov et al. (2023) analyze a closely related synthetic-only setting and similarly show that recursive training on model-generated samples leads to collapse. However, they also introduce an empirical study on what the authors denote a partial-refresh regime, in which a 10% subsample of the original real data is mixed in each iteration. This is one of the first works that show the introduction of real data can slow degradation, but in this case does not prevent it.

In a related setting, Bertrand et al. (2023) develop both a theoretical framework and empirical study to demonstrate that when a sufficiently large subsample of the original data is mixed with the synthetic data generated from the previous iteration, then model collapse can actually be entirely avoided. However, they still study the case in which no new data is added.

The above works have primarily studied the recursive training paradigm in the scope of model collapse, focusing on the potential consequences of when models are trained on

their own output. Next, we discuss works which view the recursive training paradigm as a data contamination problem, where models are trained primarily on real data, but future iterations of data may become contaminated by the synthetic output of the learned models.

Hataya et al. (2023) study a contamination setting in which a first-generation model is trained on real data and a second-generation model is trained on a mixture of the original real data and first-generation synthetic data. Their empirical results show that the second-generation model degrades relative to the first.

Extending contamination to multiple iterations, Martínez et al. (2023) keep the original real dataset fixed and add synthetic data from successive generators at each iteration. They observe empirically that this recursive contamination yields further collapse as iterations proceed. Gerstgrasser et al. (2024) provide additional empirical support for degradation under recursive contamination and give theoretical guarantees for linear models trained by least squares. They show that preserving the entire original real dataset avoids collapse, whereas replacing it with synthetic samples leads to divergence. Finally, Briesch et al. (2023) investigate an expanding data cycle for LLMs, in which each iteration *accumulates* all previous real and synthetic data, and additionally incorporates fresh real and new synthetic samples. Their experiments show that the loop maintains semantic correctness but suffers from loss of diversity, where model convergence to the true distribution is not assessed.

While these works cover a wide range of scenarios, we note that they predominately cover cases where learned generators are relatively simple, i.e. univariate Gaussian distributions, sampling procedures do not introduce new samples of real data during training iterations, or where data samples do not accumulate over all iterations. To the extent of our knowledge, no existing work provides a unifying theoretical treatment of the setting where (i) fresh real and synthetic data are sampled at each iteration, (ii) all such data are accumulated across iterations, (iii) the true data distribution does not follow any parametric assumption, and (iv) the generator is a general, potentially nonparametric, generative model. Returning to our motivating example, we note that developing such a unified framework is critical to understanding the potential consequences for example of the ever-increasing presence of AI generated output on real-world model development.

In the following section, we address this gap by developing theoretical guarantees under all four general conditions, that one may still achieve convergence, though at a new rate depending on both the baseline rate, and the fraction of real data.

### 3 Recursive Training under Data Contamination

In this section we begin by rigorously defining the generative models and the recursive training under data contamination scheme, and present theorems for the theoretical convergence under such frameworks.

**Definition 3.1** (Generative model). Let  $\mathbb{P}_0$  be the target distribution. Given a model class  $\mathcal{G}$  and a distance metric  $d$  between distributions, the goal is to learn a generative model

$G \in \mathcal{G}$  such that

$$\operatorname{argmin}_{G \in \mathcal{G}} d(G, \mathbb{P}_0).$$

Typically, one will not have access to  $\mathbb{P}_0$  directly, but rather through  $n$  i.i.d. samples from  $\mathbb{P}_0$ . In this case, while the goal of minimizing the distance remains the same, the algorithm for learning the generator will often not minimize this quantity directly as its objective but some empirical counterpart.

**Definition 3.2** (Convergence rate). Let  $\widehat{\mathbb{P}}_n$  be an estimated distribution from a generative model  $\mathcal{G}$  trained from  $n$  i.i.d. samples drawn from  $\mathbb{P}_0$ . We say that  $\widehat{\mathbb{P}}_n$  converges at a (polynomial) rate  $p > 0$  if  $d(\widehat{\mathbb{P}}_n, \mathbb{P}_0) \lesssim n^{-p}$ , i.e., there exists a constant  $C > 0$  such that  $d(\widehat{\mathbb{P}}_n, \mathbb{P}_0) \leq Cn^{-p}$ .

In this paper, when referring to setting where the model is trained with no contamination, we call the convergence rate the baseline rate. For generality, we leave the method of finding the  $\widehat{\mathbb{P}}_n$  unspecified, as our theory does not depend on the specific model but only on its convergence rate  $p$ . Moreover, if we change the notion to convergence in probability, all theorems hold in probability as well. Next, we introduce our setting of recursive training under data contamination.

**Definition 3.3** (Contaminated Recursive Training (CRT)). Let  $X_0$  be an initial dataset with  $m_1$  i.i.d. samples drawn from  $\mathbb{P}_0$ . Let the initial estimator  $\widehat{\mathbb{P}}_0$  be trained on  $X_0$ . For each step  $t \geq 1$ , perform the following operations:

1. **Recursive generation.** From the previous estimator  $\widehat{\mathbb{P}}_{t-1}$ , draw an i.i.d. synthetic sample  $Y_t$  of size  $m_2$ . Also draw a new i.i.d. real dataset  $X_t$  of size  $m_1$  from  $\mathbb{P}_0$ . Let  $\alpha := \frac{m_1}{m_1+m_2} \in (0, 1)$  be the real-data fraction.
2. **Contaminated data accumulation.** Accumulate all real datasets  $X_0, \dots, X_t$  and all previously generated synthetic datasets  $Y_1, \dots, Y_t$  into one dataset.
3. **Recursive update.** Train the learner on the accumulated data, producing the new generator  $\widehat{\mathbb{P}}_t$ .

$\{\widehat{\mathbb{P}}_t\}_{t \geq 0}$  is called the *contaminated recursively trained* (CRT) sequence of generators.

**Comparison to prior recursive training settings.** Our setup differs from the synthetic-only recursive schemes studied in the model-collapse literature (Shumailov et al., 2024, 2023; Suresh et al., 2024), where each new model is trained primarily on synthetic samples and real data from earlier rounds is discarded. Such synthetic-only recursion drives the training distribution progressively away from the target distribution and leads to collapse. Our setting also differs from replacement-style contamination models (Hataya et al., 2023), where each iteration trains on a mixture of real and synthetic data but without accumulating all past real samples. In contrast, both real and synthetic data are continuously uploaded to the internet. Additionally, internet archives retain essentially all data that has been

uploaded, both real and synthetic. Thus, it is imperative to study the setting where each iteration's generator is trained on a new sample of real data, a new sample of synthetic data from the most recent generator, and the running data from all previous iterations.

We then state the following two standard assumptions for our theoretical results.

*Assumption A1* (Polynomial rate for baseline generative models). Let  $\mathcal{Q}$  be a convex class of distributions, then there exists a constant  $0 < M < \infty$  such that for any  $\mathbb{P}_0 \in \mathcal{Q}$  the baseline generative model based on a sample of size  $n$  satisfies  $d(\hat{\mathbb{P}}_n, \mathbb{P}_0) \leq Mn^{-p}$ .

*Assumption A2* (Convex distance metric). The distance metric  $d(\cdot, \cdot)$  between distribution is convex, i.e., for any distributions  $P, Q_1, Q_2$ , and any scalars  $\lambda_1, \lambda_2 > 0$ ,

$$d(P, \lambda_1 Q_1 + \lambda_2 Q_2) \leq \lambda_1 d(P, Q_1) + \lambda_2 d(P, Q_2).$$

We emphasize that both assumptions are relatively weak in the literature and are satisfied under standard conditions commonly used in the theory of generative modeling. For example, Assumption A1 requires a uniform polynomial convergence rate over a distribution class  $\mathcal{Q}$  that is closed under convex combinations. Such uniform guarantees are classical for estimators such as kernel density estimators (KDE, Devroye, 1985) and Dirichlet process mixture models (DPMM, Ghosal and Van der Vaart, 2017). Moreover, modern deep generative models, including Variational AutoEncoders (VAE, Chérif-Abdellatif et al., 2022; Mbacke et al., 2023), Generative Adversarial Networks (GAN, Uppal et al., 2019; Puchkin et al., 2024), diffusion models (De Bortoli, 2022; Oko et al., 2023; Chen et al., 2023a; Tang et al., 2024), and certain classes of large language models (Lotfi et al., 2024; Rawat et al., 2024), are also known to satisfy such uniform convergence guarantees when the generator architecture is subject to standard regularity constraints. Finally, Assumption A2 is satisfied by most widely used statistical distances, including total variation, Kolmogorov–Smirnov, Wasserstein- $p$ , energy distance, maximum mean discrepancy (MMD), and other integral probability metrics.

With these two assumptions, we present our first main theorem about convergence rate of CRT.

**Theorem 3.4** (Convergence rate under CRT). *Suppose Assumption A1 and A2 hold. Let  $\{\hat{\mathbb{P}}_t\}_{t \geq 0}$  be the sequence of CRT learned generators, then*

$$d(\hat{\mathbb{P}}_t, \mathbb{P}_0) \lesssim \begin{cases} t^{-\alpha}, & p > \alpha, \\ t^{-\alpha} \log t, & p = \alpha, \\ t^{-p}, & p < \alpha, \end{cases}$$

Equivalently, up to logarithms,

$$d(\hat{\mathbb{P}}_t, \mathbb{P}_0) \lesssim t^{-\min\{p, \alpha\}}.$$

Additionally, if Assumption A1 is weakened to convergence in probability, the same rates hold in probability.

This theorem shows that should the real data fraction  $\alpha$  be greater than the baseline convergence rate  $p$ , then we may achieve the same convergence rate as the baseline. However, if the real data fraction  $\alpha$  is smaller than the baseline rate  $p$ , the convergence rate is slowed down. In the case where they are equal ( $p = \alpha$ ), we see a phase transition.

## 4 Biased Recursive Training under Data Contamination

In a closely related problem, we consider the case where the sampling distribution of the real data may be biased to begin with. Because generative models trained on biased datasets exhibit biased generation, this poses a significant risk in real-world settings. Furthermore, recursively contaminated training processes may further propagate errors present in the initial model stemming from this biased sampling for the training data, which subsequently poses two important questions: what happens when early model iterations are trained from biased data, and can such initially biased models be corrected in future rounds of training? We find that such questions can be studied by naturally extending our framework to the case we now refer to as biased contaminated recursive training (BCRT). In essence, one might imagine that while the original data may come from a biased source, over time these biases may be recognized and slowly corrected in the subsequent real samples. Below we study sufficient conditions on the sampling distribution in the recursive training paradigm to yield convergence as in the previous section under these circumstances.

**Definition 4.1** (Biased contaminated recursive training). Let  $(\mathbb{P}_t^{\text{bias}})_{t \geq 0}$  be a sequence of (possibly biased) distributions, and  $\mathbb{P}_0$  be our target distribution. Let  $X_0$  be an initial sample drawn from  $\mathbb{P}_0^{\text{bias}}$  and the initial estimator be  $\widehat{\mathbb{P}}_0$ . For each step  $t \geq 1$ , perform the following operations:

1. **Recursive generation.** From the previous estimator  $\widehat{\mathbb{P}}_{t-1}$ , draw an i.i.d. synthetic sample  $Y_t$  of size  $m_2$ . Also draw a i.i.d. real dataset  $X_t$  of size  $m_1$  from  $\mathbb{P}_t^{\text{bias}}$ . Let  $\alpha := \frac{m_1}{m_1 + m_2} \in (0, 1)$  be the real-data fraction.
2. **Biased contaminated data accumulation.** Accumulate all real datasets  $X_0, \dots, X_t$  and all previously generated synthetic datasets  $Y_1, \dots, Y_t$  into one dataset.
3. **Recursive update.** Train the learner on the accumulated hybrid data, producing the new generator  $\widehat{\mathbb{P}}_t$ .

The sequence  $\{\widehat{\mathbb{P}}_t\}_{t \geq 0}$  is called the *biased contaminated recursive trained* (BCRT) sequence of estimators.

As a direct consequence of Theorem 3.4, we can characterize what happens when the real samples are drawn from a fixed biased distribution and no effort is made to improve the sampling procedure or correct the bias. In this case, the recursive contamination process simply converges to the biased distribution itself. That is, the procedure will indeed “succeed,” but only in learning the biased distribution rather than the true one.

**Corollary 4.2** (Convergence to a biased distribution). *If the real datasets  $X_t$  are drawn i.i.d. from a fixed biased distribution  $\mathbb{P}_t^{\text{bias}} = \mathbb{P}_0^{\text{bias}} \neq \mathbb{P}_0$  and Assumption A1 and A2 are satisfied, then the recursive procedure converges to  $\mathbb{P}_0^{\text{bias}}$  rather than  $\mathbb{P}_0$ , with the same rates as in Theorem 3.4.*

In many realistic settings, practitioners apply bias-correction techniques or improved sampling strategies (see, e.g., (He and Garcia, 2009; Cortes and Mohri, 2014; Chen et al., 2023b) so that the real-data distribution evolves over time and gradually approaches the desired target distribution. When such corrections are applied across iterations, it is not obvious whether the recursive contamination process still converges, and if so, at what rate and to which limit. The following result addresses this setting by analyzing a biased recursive contamination process in which the real-data distributions move toward the true distribution over time. To account for this, we add an assumption on the sequence of biased distributions.

*Assumption A3* (Bias decay). The biased distributions  $\mathbb{P}_t^{\text{bias}} \in \mathcal{Q}$  and the bias decays at a polynomial rate  $q$ , i.e.,

$$d(\mathbb{P}_t^{\text{bias}}, \mathbb{P}_0) \lesssim t^{-q}.$$

This assumption captures the case where the practitioner performs any of, or any combination of: (1) improving their sampling procedures, (2) implementing bias-correction methods, or (3) working with subsequent distributions that are naturally unbiased relative to the target distribution. We note that the plausibility of this assumption in the first two cases is supported by the biased sampling and covariate shift literature, such as (He and Garcia, 2009; Cortes and Mohri, 2014; Chen et al., 2023b). We also emphasize that, in these, the rate is not necessarily determined by the model itself, but rather by the quality of the external adjustments made by the practitioner. The third case covers settings where the assumption is naturally satisfied, such as fine-tuning on a subpopulation of corpora. Additionally, the assumption that  $\mathbb{P}_t^{\text{bias}} \in \mathcal{Q}$  simply ensures that Assumption A1 applies to each of the new distributions under study. Our next result shows that Theorem 3.4 can be extended to the BCRT paradigm.

**Theorem 4.3** (Convergence rate under BCRT). *Assume that Assumptions A1, A2, and A3 hold. Let  $\{\widehat{\mathbb{P}}_t\}_{t \geq 0}$  be the sequence of BCRT learned generators, then*

$$d(\widehat{\mathbb{P}}_t, \mathbb{P}_0) \lesssim \begin{cases} t^{-\alpha}, & \min(p, q) > \alpha, \\ t^{-\alpha} \log t, & \min(p, q) = \alpha, \\ t^{-\min(p, q)}, & \min(p, q) < \alpha. \end{cases}$$

Equivalently, up to logarithms,

$$d(\widehat{\mathbb{P}}_t, \mathbb{P}_0) \lesssim t^{-\min\{p, q, \alpha\}}.$$

Like before, if either Assumption A1 or A3 are weakened to convergence in probability, the above rates hold in probability.

This theorem shows that the biased setting mirrors the unbiased case, with an additional limitation on the rate determined by how quickly the bias in the real data distribution decays.

## 5 Simulations

In this section, we construct two simulation scenarios to study the convergence rates under the CRT framework discussed in Section 3 and the BCRT framework discussed in Section 4. For CRT, we study two generative models, Kernel Density Estimation (KDE), and Wasserstein Generative Adversarial Network (WGAN), under two metrics: Wasserstein-1 Distance ( $W_1$ ) and Maximum Mean Discrepancy (MMD). We evaluate these methods in the CRT setting under different real data fractions  $\alpha = \{0.1, 0.2, \dots, 1\}$ , and compare the empirically observed rates with the predictions of Theorem 3.4 under some theoretically established base convergence rates. For BCRT, we introduce bias into the data distribution of the CRT simulation, and demonstrate the empirical convergence rates of KDE estimators under Theorem 4.3.

Table 1 summarizes a set of theoretical convergence rates for our selected generative models under various discrepancy measures. These rates rely on specific smoothness and regularity assumptions on the target distribution; details on the convergence rates for KDE and GAN may be found in Devroye (1985) and Liang (2017). Here,  $s$  denotes the Hölder smoothness for KDE and Sobolev smoothness for  $W_1$  of the true distribution and  $d$  the intrinsic dimension of the distribution’s support. In practice, the empirical rates observed in our simulations may differ from these theoretical expressions, which often guarantee only the existence of an appropriate network rather than its learnability. This gap arises because the theory does not capture the full training dynamics of modern generative models and reflects only idealized scenarios. Additionally, the values in the table should be interpreted as asymptotic rates, not as finite-sample guarantees.

| Method | $W_1$                 | MMD            |
|--------|-----------------------|----------------|
| KDE    | $-\frac{s}{2s+d}$     | $-\frac{1}{2}$ |
| WGAN   | $-\frac{s+1}{2s+2+d}$ | $-\frac{1}{2}$ |

Table 1: Theoretical convergence rate for KDE and WGAN, where  $s$  is the smoothness of the density.

Although these experiments are not intended as perfect validations, since practical issues such as optimization dynamics, overfitting, hyperparameter sensitivity, and finite sample effects can prevent models from achieving their idealized rates, we find that the empirical behavior is broadly consistent with the theoretical convergence predictions.

## 5.1 Contaminated Recursive Training (CRT)

We first consider the CRT setting from Section 3, under two different estimators: KDE with varying bandwidth, and WGAN. The density used is a mixture of two univariate Gaussians with known parameters,

$$\mathbb{P}_0 = w_1 \mathcal{N}(\mu_1, \sigma_1^2) + (1 - w_1) \mathcal{N}(\mu_2, \sigma_2^2),$$

with a density function shown in Figure 2.

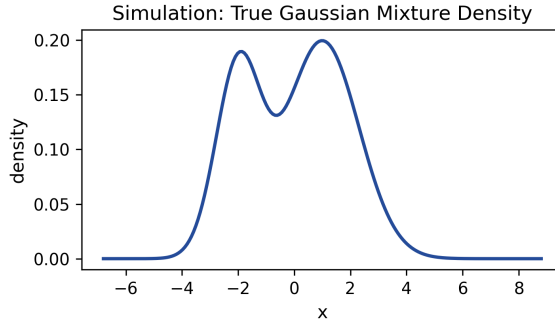


Figure 2: Density function of a two-Gaussian mixture with parameters  $w_1 = 0.35$ ,  $(\mu_1, \sigma_1) = (-2.0, 0.8)$ , and  $(\mu_2, \sigma_2) = (1.0, 1.3)$  used in Simulation of Section 5.1.

### 5.1.1 KDE with Varying Bandwidth

In the first simulation, we assess the convergence rate of the KDE estimator. We use an infinitely smooth true density as well as kernel with sufficiently quickly decaying bandwidth, so that the uncontaminated rate of  $n^{-\frac{1}{2}}$  is achieved for all metrics.

For the KDE kernel, we present two cases. The first is the standard Gaussian kernel with bandwidth set to 0, corresponding to an empirical cumulative distribution function (ECDF) estimator with known convergence rate, results shown in Figure 3. The second is the standard Gaussian kernel with a fixed initial bandwidth, following a deterministic schedule based on the sample size at each iteration, with results shown in Figure 8.

At each iteration  $t$ , we draw a new true sample of 50 real data from  $\mathbb{P}_0$  and a synthetic sample of  $\frac{1-\alpha}{\alpha}50$  from the previous model, and apply the CRT setting as in Definition 3.3. Then, either a ECDF or a KDE is used to form the next model in the sequence and the  $W_1$  loss from the ground truth is estimated by generating a sample and comparing the quantiles of the generated data to the quantiles of the true distribution on a uniform grid of 200 points. A simple linear fit to the log-log transformed data is then used to estimate the observed order of convergence. Each experiment is performed for 2000 iterations. Each experiment is repeated for 50 replicates and the mean is reported for each distance metric. The results are summarized in Figure 3, where for each  $\alpha = \{0.1, 0.2, \dots, 1\}$  and metric, the rate predicted by our theory and the rate observed in the simulation are compared.

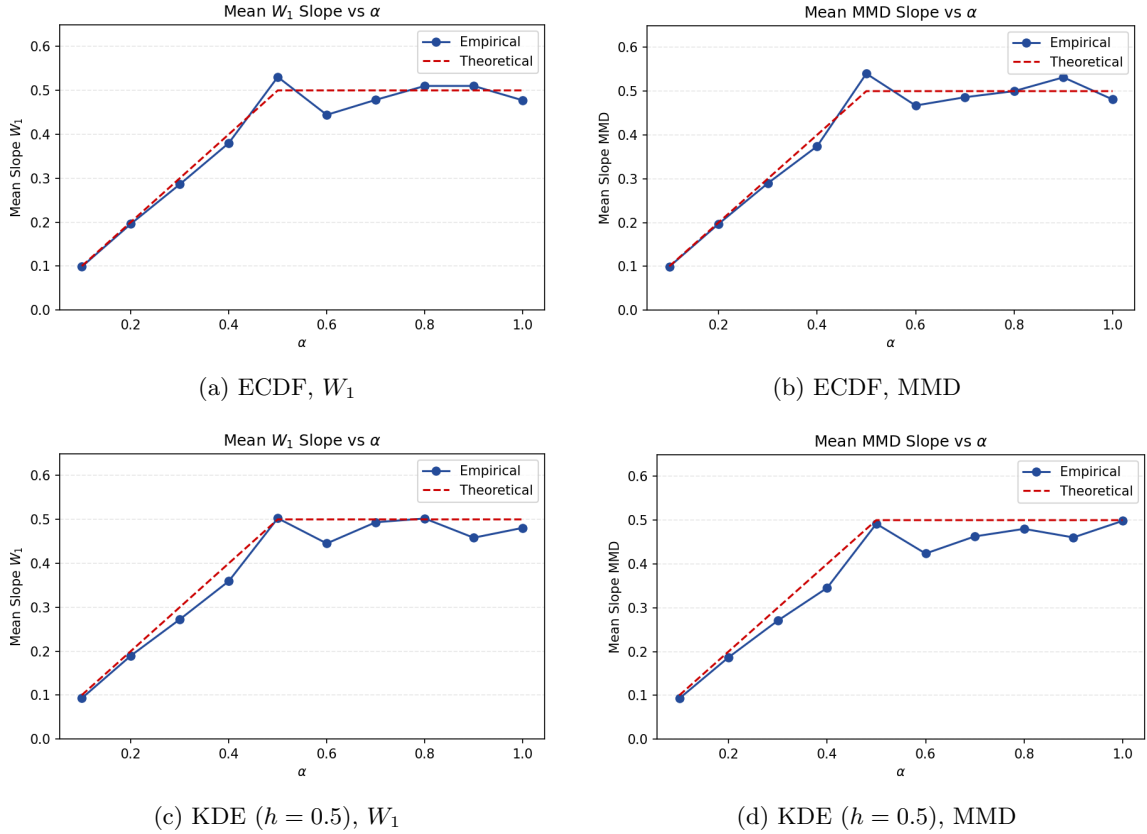


Figure 3: CRT Simulation for KDE. Top row uses an ECDF estimator (KDE with bandwidth = 0); bottom row uses KDE with initial bandwidth  $h = 0.5$ . Left column shows  $W_1$  distance, right column MMD distance with fixed bandwidth Gaussian kernel. Blue curves show empirical convergence rates while red curves show theoretical rates.

From the plots in Figure 3, we can see that the observed order of convergence is consistent with the expected order of convergence given in Theorem 3.4. Particularly, we observe that the order of convergence appears flat with respect to  $\alpha$  until the critical point ( $\alpha = p = 0.5$ ) in the phase transition is reached.

### 5.1.2 WGAN Style Generator

Here we repeat the analysis in Section 5.1.1, but replace the KDE with a generative neural network trained under  $W_1$  loss, constructed analogously to the generator network in a Wasserstein GAN. Although WGAN is a model that is typically used to learn high-dimensional distributions, in practice WGAN training is highly noisy due to the competing dual generator-critic neural network training structure Arjovsky et al. (2017); Mescheder et al. (2018). Hence, we seek to isolate the training dynamics to the architecture itself as

much as possible, replacing the critic network with an exact empirical  $W_1$  distance using the closed form sample quantile formulation.

Then at each iteration  $t$ , we draw a new true data sample from  $\mathbb{P}_0$  and a synthetic sample from the previous generator, totaling 500 new samples with fraction of real data defined by  $\alpha$ . A fresh neural network is re-initialized and trained for 25 epochs on all accumulated data. The sequence is repeated for 150 iterations for all  $\alpha$  except where  $\alpha = 0.1$ , where the number of iterations is increased to 200 to reach the asymptotic regime, and the  $W_1$  loss from the ground truth is computed by generating a new sample and comparing its quantiles to that of the ground truth over a uniform grid of 200 points. A simple linear regression on the log-log transformed data is used to estimate the rate of convergence, and each experiment is repeated for 50 replicates. The results are summarized in Figure 4, where for each  $\alpha = \{0.1, 0.2, \dots, 1\}$  and metric, the rate predicted by our theory and the rate observed in the simulation are compared.

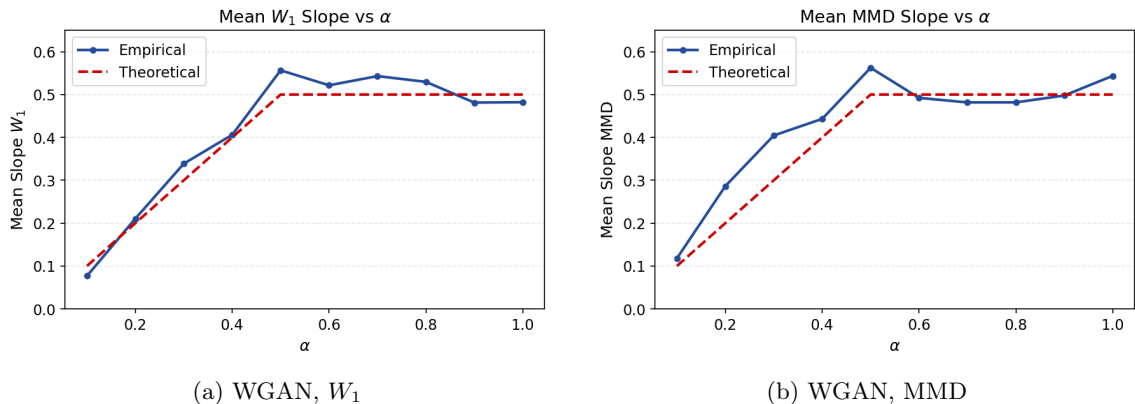


Figure 4: CRT Simulation for WGAN. Mean distributional distance for  $W_1$  (left) and MMD with fixed bandwidth Gaussian kernel (right) over 50 replicates is plotted against  $\alpha$ , the real data fraction introduced at each iteration, for  $W_1$  loss demonstrating the phase transition. In blue is the mean empirical convergence rate observed, while red indicates the theoretical rate.

We note that in many cases the empirical rate is noisy compared to the theoretical rate, likely due to training dynamics as well as practical loss floors to the optimization routines especially at the extremes of  $\alpha = 0.1$  and  $\alpha = 1.0$ . Furthermore, while the 1-dimensional  $W_1$  distance from sample quantiles is exact, there still remains statistical error from the training mini-batching, while MMD requires the choice of kernel bandwidth. However, we do find that the results are broadly consistent with rate expected from the theory.

## 5.2 Biased Recursive Training (BCRT)

We now study the BCRT framework discussed in Section 4, which combines a biased stream of real data with synthetic samples generated from the previous estimate. We omit WGAN

in this section because estimating its convergence rates is highly sensitive to hyperparameter choices. Different choices have produced rates as high as 0.5 in all cases, which is theoretically impossible, or as low as 0 when poorly tuned. With the added complexity of observation bias, it becomes difficult to separate the rate driven by the information in the data from the rate determined by hyperparameter-dependent training dynamics.

The target distribution  $\mathbb{P}_0$  is a univariate two Gaussian mixture with fixed weights and parameters, identical to that in Section 5.1.1 and Section 5.1.2. We additionally define a third Gaussian component  $\mathbb{P}_{\text{bias}} = \mathcal{N}(3, 1)$ . At each iteration, a biased real data sample of size 50 is drawn from  $\mathbb{P}_t^{\text{bias}} = (1 - \text{bias}_t)\mathbb{P}_0 + \text{bias}_t\mathbb{P}_{\text{bias}}$ , and a sample of  $\frac{1-\alpha}{\alpha}50$  synthetic data is sampled from the previous iteration’s fitted model. We note the contamination level decays over time at a polynomial rate governed by a parameter  $q$ , that is  $\text{bias}_t \asymp t^{-q}$ , so that Assumption A3 is satisfied. Then, either an ECDF or a KDE is used to form the next model in the sequence and the  $W_1$  loss from the ground truth is computed in a manner identical to Section 3. As before, a simple linear fit to the log-log transformed data estimates the rate of convergence, each experiment is performed for 2000 iterations and 100 and 20 replicates for ECDF and KDE respectively. The experiment is performed for each combination of  $\alpha = \{0.25, 0.5, 0.75\}$  and  $q = \{0.25, 0.5, 0.75\}$ . Because we now vary over two experimental parameters,  $\alpha$  and  $q$ , we reduce the number of parameters and present the results in a table below for concision.

Table 2 shows that the empirical rates match our theoretical rates in Theorem 4.3 under the BCRT framework.

| Parameters |       |        | Empirical CDF |       | KDE   |       |
|------------|-------|--------|---------------|-------|-------|-------|
| $\alpha$   | $q$   | Theory | $W_1$         | MMD   | $W_1$ | MMD   |
| 0.250      | 0.250 | 0.250  | 0.207         | 0.226 | 0.183 | 0.172 |
| 0.250      | 0.500 | 0.250  | 0.234         | 0.242 | 0.223 | 0.194 |
| 0.250      | 0.750 | 0.250  | 0.247         | 0.245 | 0.215 | 0.191 |
| 0.500      | 0.250 | 0.250  | 0.325         | 0.421 | 0.332 | 0.330 |
| 0.750      | 0.250 | 0.250  | 0.232         | 0.319 | 0.257 | 0.284 |
| 0.500      | 0.500 | 0.500  | 0.506         | 0.517 | 0.452 | 0.408 |
| 0.500      | 0.750 | 0.500  | 0.535         | 0.534 | 0.461 | 0.409 |
| 0.750      | 0.500 | 0.500  | 0.473         | 0.487 | 0.467 | 0.440 |
| 0.750      | 0.750 | 0.500  | 0.482         | 0.502 | 0.484 | 0.416 |

Table 2: BCRT Simulation, (KDE, initial bandwidth = 2.0). Mean distributional distance over 100 replicates for ECDF and 20 replicates for KDE. Theoretical values are provided alongside estimated convergence rates for  $W_1$  loss and MMD.

## 6 Real Data Experiments

Thus far we have demonstrated the empirical rates of convergence under CRT and BCRT in simulated environments, using multiple models, where the true distribution  $\mathbb{P}_0$  is known, and where we have an exact empirical formulation of  $W_1$  using quantiles in 1 dimension.

We now consider a more realistic data scenario, training a state of the art diffusion model on MNIST images. Although diffusion models have a known rate of convergence under  $W_1$  loss which fits into the CRT framework of Section 3, in practice it is difficult to observe the precise predicted rates due to complex neural network training dynamics, a significant number of hyperparameters in the diffusion architecture, as well as not having an exact  $W_1$  metric in greater than 1 dimension. Furthermore, in realistic high-dimensional data scenarios such as with images, we do not know the ground truth distribution  $\mathbb{P}_0$ . Hence, in this section we focus on using a diffusion network and the MNIST dataset to demonstrate that under CRT of Section 3, such generative models can still converge notably even when the fraction of real data added in each iteration is less than 0.5. In other words, even under significant data contamination during recursive training, we find that the generative models still converge as in Theorem 3.4.

In each iteration, a total of 300 images is chosen, with fraction  $\alpha$  drawn from the MNIST dataset without replacement, and a synthetic sample of fraction  $1 - \alpha$  images is generated by the generator trained in the previous iteration. The network is trained for exactly 150 epochs on the current training data, and the sequence is repeated for 300 total iterations. In this case, the data accumulates through the optimizer, through which the data is used an equal number of times per real training sample accordant with Theorem 3.4, and the model is not reinitialized at each iteration. Finally, due to the high dimensionality of the image space,  $W_1$  distances are not evaluated.

In Figure 5, we illustrate the CRT training procedure with input training data at each iteration, and in Figure 6 we present sample outputs of the learned generator at different iterations. These results empirically verify that even when  $\alpha < 1$ , the diffusion model under CRT tends to converge.

## 7 Discussion and Future Work

In this article, we have analyzed the behavior of generative models trained under the contaminated recursive training (CRT) framework, where each training iteration mixes fresh real data with synthetic data produced by previous model iterations. We have established convergence guarantees for this setting, showing that the convergence rate of the recursively learned distribution is governed by a phase transition: it is limited by the minimum of (i) the baseline convergence rate and (ii) the real-data fraction. We further extended the analysis to the case in which the real data itself is drawn from a sequence of biased distributions, and proved that convergence to the true distribution is still possible provided the sequence of real-data distributions approaches the target distribution. In this setting, the same phase transition appears, with an additional term corresponding to the decay of the bias.

Our results illustrate that both CRT and BCRT may slow the baseline convergence rate, but neither phenomenon is inherently catastrophic. The quantity and quality of real data directly determine the resulting convergence rate, giving a precise formulation of the effect of recursive contamination. Importantly, the theory suggests that bias-reduction efforts,

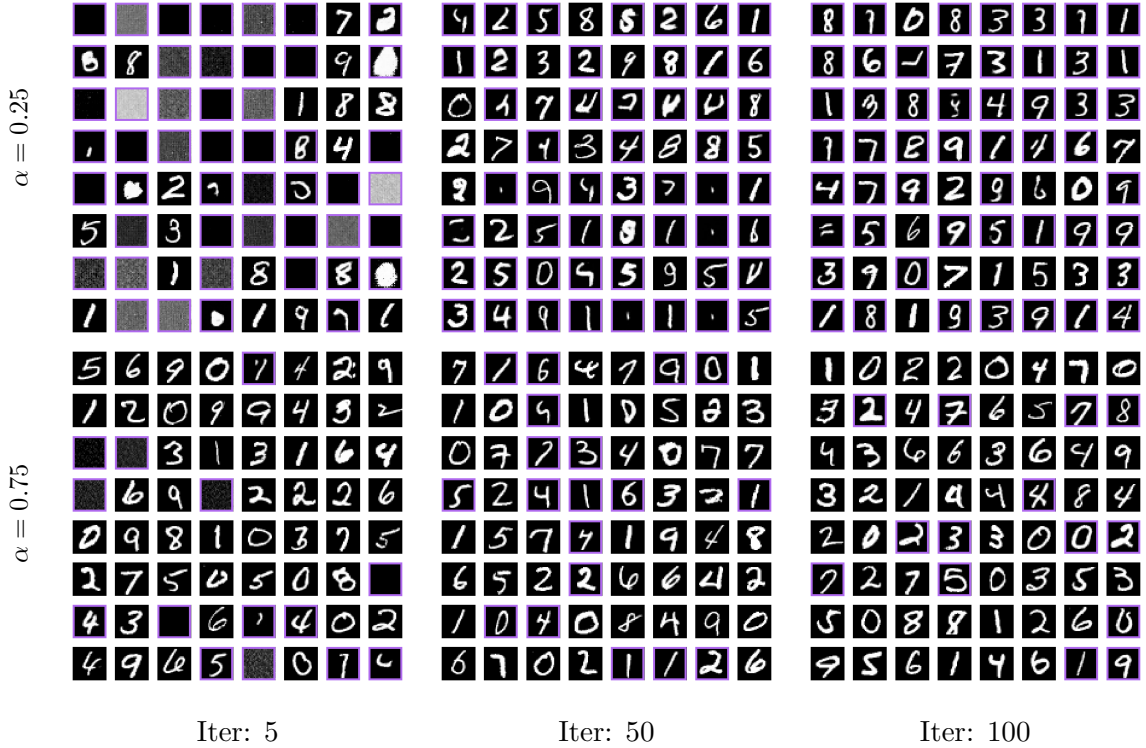


Figure 5: Diffusion model trained under CRT on MNIST with fraction of real data  $\alpha = \{0.25, 0.75\}$ . Examples of input training data at each iteration, with synthetic generated data highlighted in purple.

such as improved data collection or filtering, sampling corrections, and debiasing methods, remain valuable even when the generative AI models were originally trained on imperfect or biased data. There are, however, several directions for future work.

First, online content is not sampled uniformly from a generator: human users or automated agents choose prompts, selectively edit outputs, and decide which generations to publish. For example high-quality text (e.g., scientific writing) undergoes substantial human filtering before being introduced to the internet, which may lead to only particularly “good” samples from each model iteration becoming part of the corpora. Meanwhile low-quality or harmful outputs (e.g., toxic or misleading content) may be purposely amplified by malicious actors, such as for misinformation campaigns or trolling, leading to inflated quantities of particularly harmful corpora. These selection mechanisms are not modeled here and present an important area of future research.

Second, modern large-scale training pipelines employ curated datasets, reinforcement learning from human feedback, professional annotation, and substantial quality-control infrastructure. These processes are not captured in the CRT setting. Moreover, contemporary generative models are often trained not merely to approximate a data distribution but to

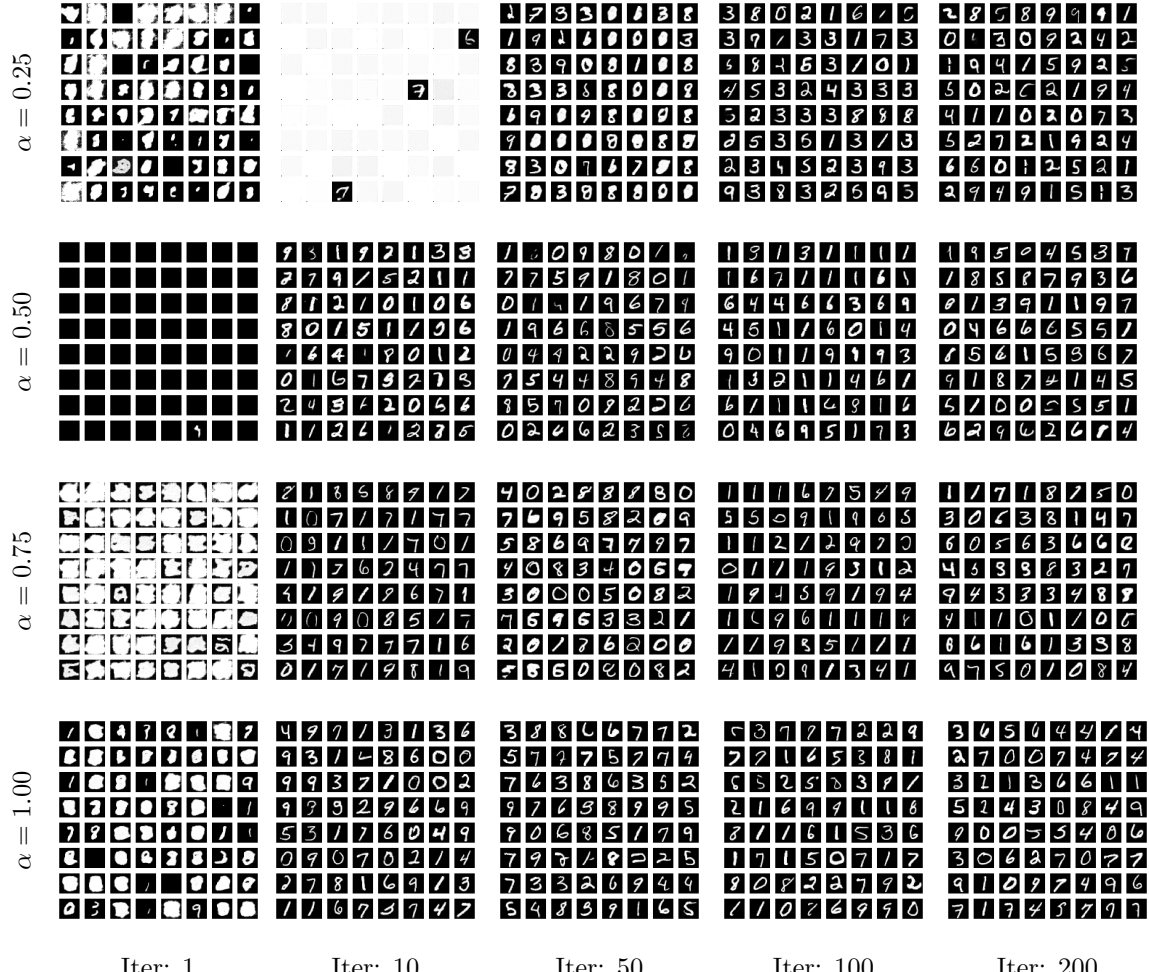


Figure 6: Diffusion model trained under CRT on MNIST with fraction of real data  $\alpha = \{0.25, 0.50, 0.75, 1.00\}$ . Samples of generated images from learned model at different CRT iterations indicate model convergence in all cases.

optimize a reward signal or graded evaluation of their outputs, often supplied by human annotators, automated evaluators, or learned reward models (reinforcement learning from human feedback and supervised fine tuning). In such systems, distribution learning is a byproduct rather than the primary objective, and the effective training dynamics may differ from those assumed in our framework. Extending the theory to incorporate these more realistic forms of selection, curation, and reinforcement is an important direction for future work.

Third, we note that many important classes of loss, such as cross-entropy, likelihood, and Kullback-Leibler, do not satisfy the requirements of our theory. Extending the proof from our metric assumptions to include these losses is an important step forwards in un-

derstanding the behavior of LLMs in the CRT setting.

Finally, we note that a substantial literature leverages the intentional use of synthetic data for training. In data-scarce settings, training on synthetic data has enabled models to achieve strong performance on real data, both after subsequent retraining and, in some cases, even without further adaptation. In some settings, models are trained entirely on data generated from computer simulation and then deployed in the physical world with little or no additional real-world training, such as in reinforcement learning with low tolerance for negative outcomes, such as controlling vehicles Sadeghi and Levine (2016). An important direction for future work is to extend our analysis to settings where synthetic data is deliberately introduced due to limited real data availability, and where one can control where, when, and how much synthetic data is incorporated.

Synthetic data also plays a central role in privacy-sensitive applications. In such settings, generated data is often used as a surrogate for real data to preserve anonymity, after which it supports downstream tasks such as effect estimation, model training, or federated learning. This makes it critical to understand how approximation errors in the generator propagate into the synthetic dataset and subsequently impact downstream inference and learning.

Moreover, synthetic data is not the only way that error in one learned model may propagate to downstream models. For example, knowledge distillation replaces hard labels with teacher-generated targets (Hinton et al., 2015; Furlanello et al., 2018). Many LLMs now come with mini models distilled from larger models, rather than trained solely on the same datasets as those larger models Sanh et al. (2019). Understanding the long-term statistical effects of propagating errors through models during distillation is also an important future direction.

## References

- Eric Arazo, Diego Ortego, Paul Albert, Noel E O’Connor, and Kevin McGuinness. Pseudo-labeling and confirmation bias in deep semi-supervised learning. In *2020 International joint conference on neural networks (IJCNN)*, pages 1–8. IEEE, 2020.
- Martin Arjovsky, Soumith Chintala, and Léon Bottou. Wasserstein generative adversarial networks. In *International conference on machine learning*, pages 214–223. PMLR, 2017.
- BBC News. Bbc reveals web of spammers profiting from ai holocaust images, August 2025. URL <https://www.bbc.com/news/articles/ckg4xjk1g1xo>. Retrieved November 3, 2025.
- Quentin Bertrand, Avishek Joey Bose, Alexandre Duplessis, Marco Jiralerpong, and Gauthier Gidel. On the stability of iterative retraining of generative models on their own data. *arXiv preprint arXiv:2310.00429*, 2023.
- Benjamin Billot, Douglas N Greve, Oula Puonti, Axel Thielscher, Koen Van Leemput, Bruce Fischl, Adrian V Dalca, Juan Eugenio Iglesias, et al. Synthseg: Segmentation of

brain mri scans of any contrast and resolution without retraining. *Medical image analysis*, 86:102789, 2023.

Christopher Bowles, Liang Chen, Ricardo Guerrero, Paul Bentley, Roger Gunn, Alexander Hammers, David Alexander Dickie, Maria Valdés Hernández, Joanna Wardlaw, and Daniel Rueckert. Gan augmentation: Augmenting training data using generative adversarial networks. *arXiv preprint arXiv:1810.10863*, 2018.

Martin Briesch, Dominik Sobania, and Franz Rothlauf. Large language models suffer from their own output: An analysis of the self-consuming training loop. 2023.

Creston Brooks, Samuel Eggert, and Denis Peskoff. The rise of ai-generated content in wikipedia. *arXiv preprint arXiv:2410.08044*, 2024.

Minshuo Chen, Kaixuan Huang, Tuo Zhao, and Mengdi Wang. Score approximation, estimation and distribution recovery of diffusion models on low-dimensional data. In *International Conference on Machine Learning*, pages 4672–4712. PMLR, 2023a.

Zhenpeng Chen, Jie M Zhang, Federica Sarro, and Mark Harman. A comprehensive empirical study of bias mitigation methods for machine learning classifiers. *ACM transactions on software engineering and methodology*, 32(4):1–30, 2023b.

Badr-Eddine Chérief-Abdellatif, Yuyang Shi, Arnaud Doucet, and Benjamin Guedj. On pac-bayesian reconstruction guarantees for vaes. In *International conference on artificial intelligence and statistics*, pages 3066–3079. PMLR, 2022.

Corinna Cortes and Mehryar Mohri. Domain adaptation and sample bias correction theory and algorithm for regression. *Theoretical Computer Science*, 519:103–126, 2014.

James L Cross, Michael A Choma, and John A Onofrey. Bias in medical ai: Implications for clinical decision-making. *PLOS Digital Health*, 3(11):e0000651, 2024.

Valentin De Bortoli. Convergence of denoising diffusion models under the manifold hypothesis. *arXiv preprint arXiv:2208.05314*, 2022.

Luc Devroye. Nonparametric density estimation. *The L\_1 View*, 1985.

Rémi Flamary, Nicolas Courty, Alexandre Gramfort, Mokhtar Z Alaya, Aurélie Boisbunon, Stanislas Chambon, Laetitia Chapel, Adrien Corenflos, Kilian Fatras, Nemo Fournier, et al. Pot: Python optimal transport. *The Journal of Machine Learning Research*, 22(1): 3571–3578, 2021.

Nicole Froio. Ai is ruining houseplant communities online, June 2025.  
URL <https://www.theverge.com/ai-artificial-intelligence/691355/ai-is-ruining-houseplant-communities-online>. Accessed: 2025-06-26.

Tommaso Furlanello, Zachary Lipton, Michael Tschannen, Laurent Itti, and Anima Anandkumar. Born again neural networks. In *International conference on machine learning*, pages 1607–1616. PMLR, 2018.

Walter Gautschi. Some elementary inequalities relating to the gamma and incomplete gamma function. *J. Math. Phys.*, 38(1):77–81, 1959.

Matthias Gerstgrasser, Rylan Schaeffer, Apratim Dey, Rafael Rafailov, Henry Sleight, John Hughes, Tomasz Korbak, Rajashree Agrawal, Dhruv Pai, Andrey Gromov, et al. Is model collapse inevitable? breaking the curse of recursion by accumulating real and synthetic data. *arXiv preprint arXiv:2404.01413*, 2024.

Subhashis Ghosal and Aad W Van der Vaart. *Fundamentals of nonparametric Bayesian inference*, volume 44. Cambridge University Press, 2017.

Ryuichiro Hataya, Han Bao, and Hiromi Arai. Will large-scale generative models corrupt future datasets? In *Proceedings of the IEEE/CVF International Conference on Computer Vision*, pages 20555–20565, 2023.

Haibo He and Edwardo A Garcia. Learning from imbalanced data. *IEEE Transactions on knowledge and data engineering*, 21(9):1263–1284, 2009.

Geoffrey Hinton, Oriol Vinyals, and Jeff Dean. Distilling the knowledge in a neural network. *arXiv preprint arXiv:1503.02531*, 2015.

James Jordon, Jinsung Yoon, and Mihaela Van Der Schaar. Pate-gan: Generating synthetic data with differential privacy guarantees. In *International conference on learning representations*, 2018.

Dong-Hyun Lee et al. Pseudo-label: The simple and efficient semi-supervised learning method for deep neural networks.

Tengyuan Liang. How well can generative adversarial networks learn densities: A nonparametric view. *arXiv preprint arXiv:1712.08244*, 2017.

Weixin Liang, Zachary Izzo, Yaohui Zhang, Haley Lepp, Hancheng Cao, Xuandong Zhao, Lingjiao Chen, Haotian Ye, Sheng Liu, Zhi Huang, et al. Monitoring ai-modified content at scale: A case study on the impact of chatgpt on ai conference peer reviews. *PMLR*, 2024.

Raphael Gontijo Lopes, Stefano Fenu, and Thad Starner. Data-free knowledge distillation for deep neural networks. *arXiv preprint arXiv:1710.07535*, 2017.

Sanae Lotfi, Yilun Kuang, Marc Finzi, Brandon Amos, Micah Goldblum, and Andrew G Wilson. Unlocking tokens as data points for generalization bounds on larger language models. *Advances in Neural Information Processing Systems*, 37:9229–9256, 2024.

- Li Lucy and David Bamman. Gender and representation bias in gpt-3 generated stories. In *Proceedings of the third workshop on narrative understanding*, pages 48–55, 2021.
- Gonzalo Martínez, Lauren Watson, Pedro Reviriego, José Alberto Hernández, Marc Juarez, and Rik Sarkar. Combining generative artificial intelligence (ai) and the internet: Heading towards evolution or degradation? *arXiv preprint arXiv:2303.01255*, 2023.
- Sokhna Diarra Mbacke, Florence Clerc, and Pascal Germain. Statistical guarantees for variational autoencoders using pac-bayesian theory. *Advances in Neural Information Processing Systems*, 36:56903–56915, 2023.
- Ninareh Mehrabi, Fred Morstatter, Nripsuta Saxena, Kristina Lerman, and Aram Galstyan. A survey on bias and fairness in machine learning. *ACM computing surveys (CSUR)*, 54(6):1–35, 2021.
- Lars Mescheder, Andreas Geiger, and Sebastian Nowozin. Which training methods for gans do actually converge? In *International conference on machine learning*, pages 3481–3490. PMLR, 2018.
- Kazusato Oko, Shunta Akiyama, and Taiji Suzuki. Diffusion models are minimax optimal distribution estimators. In *International Conference on Machine Learning*, pages 26517–26582. PMLR, 2023.
- Nicolas Papernot, Martín Abadi, Ulfar Erlingsson, Ian Goodfellow, and Kunal Talwar. Semi-supervised knowledge transfer for deep learning from private training data. *arXiv preprint arXiv:1610.05755*, 2016.
- Nikita Puchkin, Sergey Samsonov, Denis Belomestny, Eric Moulines, and Alexey Naumov. Rates of convergence for density estimation with generative adversarial networks. *Journal of Machine Learning Research*, 25(29):1–47, 2024.
- Ankit Singh Rawat, Veeranjaneyulu Sadhanala, Afshin Rostamizadeh, Ayan Chakrabarti, Wittawat Jitkrittum, Vladimir Feinberg, Seungyeon Kim, Hrayr Harutyunyan, Nikunj Saunshi, Zachary Nado, et al. A little help goes a long way: Efficient llm training by leveraging small lms. *arXiv preprint arXiv:2410.18779*, 2024.
- Walter Rudin. Principles of mathematical analysis. 3rd ed., 1976.
- Fereshteh Sadeghi and Sergey Levine. Cad2rl: Real single-image flight without a single real image. *arXiv preprint arXiv:1611.04201*, 2016.
- Victor Sanh, Lysandre Debut, Julien Chaumond, and Thomas Wolf. Distilbert, a distilled version of bert: smaller, faster, cheaper and lighter. *arXiv preprint arXiv:1910.01108*, 2019.

Emily Sheng, Kai-Wei Chang, Prem Natarajan, and Nanyun Peng. The woman worked as a babysitter: On biases in language generation. In *Proceedings of the 2019 conference on empirical methods in natural language processing and the 9th international joint conference on natural language processing (EMNLP-IJCNLP)*, pages 3407–3412, 2019.

Ilia Shumailov, Zakhar Shumaylov, Yiren Zhao, Yarin Gal, Nicolas Papernot, and Ross Anderson. The curse of recursion: Training on generated data makes models forget. *arXiv preprint arXiv:2305.17493*, 2023.

Ilia Shumailov, Zakhar Shumaylov, Yiren Zhao, Nicolas Papernot, Ross Anderson, and Yarin Gal. Ai models collapse when trained on recursively generated data. *Nature*, 631(8022):755–759, 2024.

Ananda Theertha Suresh, Andrew Thangaraj, and Aditya Nanda Kishore Khandavally. Rate of model collapse in recursive training. *arXiv preprint arXiv:2412.17646*, 2024.

Rong Tang, Lizhen Lin, and Yun Yang. Conditional diffusion models are minimax-optimal and manifold-adaptive for conditional distribution estimation. *arXiv preprint arXiv:2409.20124*, 2024.

Josh Tobin, Rachel Fong, Alex Ray, Jonas Schneider, Wojciech Zaremba, and Pieter Abbeel. Domain randomization for transferring deep neural networks from simulation to the real world. In *2017 IEEE/RSJ international conference on intelligent robots and systems (IROS)*, pages 23–30. IEEE, 2017.

Ananya Uppal, Shashank Singh, and Barnabás Póczos. Nonparametric density estimation & convergence rates for gans under besov ipm losses. *Advances in neural information processing systems*, 32, 2019.

Liyang Xie, Kaixiang Lin, Shu Wang, Fei Wang, and Jiayu Zhou. Differentially private generative adversarial network. *arXiv preprint arXiv:1802.06739*, 2018.

Qizhe Xie, Minh-Thang Luong, Eduard Hovy, and Quoc V Le. Self-training with noisy student improves imagenet classification. In *Proceedings of the IEEE/CVF conference on computer vision and pattern recognition*, pages 10687–10698, 2020.

Hongxu Yin, Pavlo Molchanov, Jose M Alvarez, Zhizhong Li, Arun Mallya, Derek Hoiem, Niraj K Jha, and Jan Kautz. Dreaming to distill: Data-free knowledge transfer via deep-inversion. In *Proceedings of the IEEE/CVF conference on computer vision and pattern recognition*, pages 8715–8724, 2020.

Mi Zhou, Vibhanshu Abhishek, Timothy Derdenger, Jaymo Kim, and Kannan Srinivasan. Bias in generative ai. *arXiv preprint arXiv:2403.02726*, 2024.

## A Code Availability

All code to run simulations, experiments, and to generate all figures are available at: <https://github.com/hong-niu/generative-recursive-training>.

## B Proofs

In this section we provide the proofs for Theorem 3.4 and Theorem 4.3.

### B.1 Proof of Theorem 3.4

*Proof.* Define

$$\mathbb{Q}_t = \frac{1}{M_t} \left[ tm_1 \mathbb{P}_0 + \sum_{j=1}^{t-1} m_2 \hat{\mathbb{P}}_j \right], \quad M_t = tm_1 + (t-1)m_2.$$

Using Assumptions A1 and A2, we obtain We first use the triangle inequality to write

$$d(\hat{\mathbb{P}}_t, \mathbb{P}_0) \leq d(\hat{\mathbb{P}}_t, \mathbb{Q}_t) + d(\mathbb{Q}_t, \mathbb{P}_0).$$

To treat  $d(\hat{\mathbb{P}}_t, \mathbb{Q}_t)$ , note that  $\hat{\mathbb{P}}_t$  is learned from the accumulated data whose distribution is  $\mathbb{Q}_t$ . Using A1, which states that the baseline generative model has a uniform polynomial rate  $p$ , we may treat  $\mathbb{Q}_t$  as the distribution to be learned by  $\hat{\mathbb{P}}_t$  at iteration  $t$ , yielding  $d(\hat{\mathbb{P}}_t, \mathbb{Q}_t) \lesssim M_t^{-p}$ . Then we may write

$$d(\hat{\mathbb{P}}_t, \mathbb{P}_0) \leq d(\hat{\mathbb{P}}_t, \mathbb{Q}_t) + d(\mathbb{Q}_t, \mathbb{P}_0) \lesssim M_t^{-p} + d(\mathbb{Q}_t, \mathbb{P}_0).$$

From assumption A2, by convexity of  $d$  in its second argument,

$$\begin{aligned} d(\mathbb{Q}_t, \mathbb{P}_0) &= d\left(\mathbb{P}_0, \frac{tm_1}{M_t} \mathbb{P}_0 + \frac{m_2}{M_t} \sum_{j=1}^{t-1} \hat{\mathbb{P}}_j\right) \\ &\leq \frac{tm_1}{M_t} d(\mathbb{P}_0, \mathbb{P}_0) + \frac{m_2}{M_t} \sum_{j=1}^{t-1} d(\mathbb{P}_0, \hat{\mathbb{P}}_j) \\ &= \frac{m_2}{M_t} \sum_{j=1}^{t-1} d(\mathbb{P}_0, \hat{\mathbb{P}}_j). \end{aligned}$$

Thus

$$d(\hat{\mathbb{P}}_t, \mathbb{P}_0) \lesssim M_t^{-p} + \frac{m_2}{M_t} \sum_{j=1}^{t-1} d(\mathbb{P}_0, \hat{\mathbb{P}}_j). \quad (1)$$

Let  $S_{t-1} := \sum_{j=1}^{t-1} d(\mathbb{P}_0, \widehat{\mathbb{P}}_j)$ . Applying (1) at step  $t-1$  gives

$$d(\widehat{\mathbb{P}}_{t-1}, \mathbb{P}_0) \lesssim M_{t-1}^{-p} + \frac{m_2}{M_{t-1}} S_{t-2},$$

so

$$\begin{aligned} S_{t-1} &= d(\widehat{\mathbb{P}}_{t-1}, \mathbb{P}_0) + S_{t-2} \\ &\lesssim M_{t-1}^{-p} + \left(1 + \frac{m_2}{M_{t-1}}\right) S_{t-2}. \end{aligned}$$

Iterating this recursion yields

$$S_{t-1} \lesssim M_{t-1}^{-p} + \sum_{j=1}^{t-2} M_j^{-p} \prod_{k=j}^{t-2} \left(1 + \frac{m_2}{M_k}\right).$$

Substituting back into (1) gives

$$d(\widehat{\mathbb{P}}_t, \mathbb{P}_0) \lesssim M_t^{-p} + \frac{m_2}{M_t} M_{t-1}^{-p} + \frac{m_2}{M_t} \sum_{j=1}^{t-2} M_j^{-p} \prod_{k=j}^{t-2} \left(1 + \frac{m_2}{M_k}\right).$$

Since

$$M_t = tm_1 + (t-1)m_2 = (m_1 + m_2)t - m_2,$$

we have  $M_t \asymp (m_1 + m_2)t$ , hence there exist constants  $c_1, c_2 > 0$  such that

$$c_1(m_1 + m_2)t \leq M_t \leq c_2(m_1 + m_2)t \quad \text{for all } t \geq 1.$$

Similarly,

$$M_t^{-p} \lesssim (m_1 + m_2)^{-p} t^{-p}, \quad \frac{m_2}{M_t} \lesssim \frac{1-\alpha}{t},$$

with  $\alpha = m_1/(m_1 + m_2)$ , and similarly  $M_j^{-p} \lesssim (m_1 + m_2)^{-p} j^{-p}$ . Thus

$$\begin{aligned} d(\widehat{\mathbb{P}}_t, \mathbb{P}_0) &\lesssim (m_1 + m_2)^{-p} t^{-p} + m_2(m_1 + m_2)^{-p-1} (t-1)^{-p-1} \\ &\quad + (1-\alpha)t^{-1}(m_1 + m_2)^{-p} \sum_{j=1}^{t-2} j^{-p} \prod_{k=j}^{t-2} \left(1 + \frac{1-\alpha}{k}\right) \end{aligned} \tag{2}$$

$$\lesssim t^{-p} + t^{-p-1} + t^{-1} \sum_{j=1}^{t-2} j^{-p} \prod_{k=j}^{t-2} \left(1 + \frac{1-\alpha}{k}\right). \tag{3}$$

We now analyze the last term (without constants) in Equation (3):

$$\begin{aligned}
t^{-1} \sum_{j=1}^{t-2} j^{-p} \prod_{k=j}^{t-2} \left(1 + \frac{1-\alpha}{k}\right) &= \sum_{j=1}^{t-2} j^{-p} t^{-1} \left[ \prod_{k=j}^{t-2} \left(\frac{k+1-\alpha}{k}\right) \right] \\
&= \sum_{j=1}^{t-2} j^{-p} t^{-1} \frac{t-1}{j} \left[ \prod_{k=j}^{t-2} \left(\frac{k+1-\alpha}{k}\right) \left(\frac{k}{k+1}\right) \right] \\
&= \sum_{j=1}^{t-2} j^{-p} \left(\frac{t-1}{t}\right) j^{-1} \left[ \prod_{k=j}^{t-2} \left(\frac{k+1-\alpha}{k+1}\right) \right],
\end{aligned}$$

where we use the identity  $\prod_{k=j}^{t-2} \frac{k}{k+1} = \frac{j}{t-1}$ . Using the Gamma function, we have the exact identity

$$\prod_{k=j}^{t-2} \left(\frac{k+1-\alpha}{k+1}\right) = \frac{\Gamma(t+1-\alpha-1)}{\Gamma(j+1-\alpha)} \frac{\Gamma(j+1)}{\Gamma(t)} = \frac{\Gamma(t-\alpha)}{\Gamma(j+1-\alpha)} \frac{\Gamma(j+1)}{\Gamma(t)}.$$

We now recall the following standard inequalities for the Gamma function.

**Gamma bounds.** For  $x > 0$  and  $0 < s < 1$ , Gautschi's inequality (Gautschi, 1959) states that

$$x^{1-s} < \frac{\Gamma(x+1)}{\Gamma(x+s)} < (x+1)^{1-s}.$$

Combined with Stirling-type bounds for  $\Gamma$  (Rudin, 1976), this implies that for any  $\alpha \in (0, 1)$  there exist constants  $c_1, c_2, c_3, c_4 > 0$  such that for all integers  $t, j \geq 1$ ,

$$c_1 t^{-\alpha} \leq \frac{\Gamma(t-\alpha)}{\Gamma(t)} \leq c_2 t^{-\alpha}, \quad c_3 j^\alpha \leq \frac{\Gamma(j+1)}{\Gamma(j+1-\alpha)} \leq c_4 j^\alpha. \quad (4)$$

Using (4), the contribution of the last term (without constants) in Equation (3) is bounded by

$$\left(\frac{t-1}{t}\right) \frac{\Gamma(t-\alpha)}{\Gamma(t)} \sum_{j=1}^{t-2} j^{-p-1} \frac{\Gamma(j+1)}{\Gamma(j+1-\alpha)} \lesssim t^{-\alpha} \sum_{j=1}^{t-2} j^{-p-1+\alpha}.$$

Putting all terms together, we have shown that

$$d(\widehat{\mathbb{P}}_t, \mathbb{P}_0) \lesssim t^{-p} + (t-1)^{-p-1} + t^{-\alpha} \sum_{j=1}^{t-2} j^{-p-1+\alpha}. \quad (5)$$

Finally, we use the standard bounds for p-series:

$$\sum_{j=1}^{t-2} j^{-1-(p-\alpha)} \lesssim \begin{cases} 1, & p > \alpha, \\ \log t, & p = \alpha, \\ t^{\alpha-p}, & p < \alpha. \end{cases}$$

We now treat the three regimes separately, always absorbing the first two terms of (5) into the dominant term by adjusting the constant if needed.

**Case 1:**  $p > \alpha$ . Then  $\sum_{j=1}^{t-2} j^{-p-(1-\alpha)} \lesssim 1$ , so the third term in (5) is

$$\lesssim t^{-\alpha}.$$

Moreover, since  $p > \alpha$  we have  $t^{-p} \leq t^{-\alpha}$  for all  $t \geq 1$ , and

$$(t-1)^{-p-1} \lesssim t^{-p-1} \leq t^{-p} \leq t^{-\alpha}.$$

Hence, all three terms in (5) are asymptotically bounded by  $t^{-\alpha}$ , and therefore

$$d(\widehat{\mathbb{P}}_t, \mathbb{P}_0) \lesssim t^{-\alpha}.$$

**Case 2:**  $p = \alpha$ . Then  $\sum_{j=1}^{t-2} j^{-p-(1-\alpha)} = \sum_{j=1}^{t-2} j^{-1} \lesssim \log t$ , and  $t^{-p} = t^{-\alpha}$ . Thus the third term in (5) is

$$\lesssim t^{-\alpha} \log t.$$

The first term in (5) is  $t^{-p}$ , which is dominated by  $t^{-p} \log t$ , and the second term  $(t-1)^{-p-1}$  is of strictly smaller order. Therefore

$$d(\widehat{\mathbb{P}}_t, \mathbb{P}_0) \lesssim t^{-\alpha} \log t.$$

**Case 3:**  $p < \alpha$ . Then

$$\sum_{j=1}^{t-2} j^{-1-(p-\alpha)} \lesssim t^{1-1-(p-\alpha)} = t^{\alpha-p}.$$

Hence the third term in (5) is

$$t^{-\alpha} t^{\alpha-p} = t^{-p}.$$

The first term  $t^{-p}$  and the second term  $(t-1)^{-p-1}$  are dominated by the third term still, so all three terms are  $O(t^{-p})$  up to multiplicative constants. Therefore

$$d(\widehat{\mathbb{P}}_t, \mathbb{P}_0) \lesssim t^{-p}.$$

Combining the three cases, we have proved that

$$d(\widehat{\mathbb{P}}_t, \mathbb{P}_0) \lesssim \begin{cases} t^{-\alpha}, & p > \alpha, \\ t^{-\alpha} \log t, & p = \alpha, \\ t^{-p}, & p < \alpha. \end{cases}$$

If one observes that if assumption A1 holds in probability, all  $\lesssim$  hold in probability, and we have Theorem 3.4. □

## B.2 Proof of Theorem 4.3

We first show the following lemma that will be useful in our later proofs.

**Lemma B.1** (Cesàro rate for drifting distributions). *Let  $d(\cdot, \cdot)$  be a metric on distributions that is convex in its second argument. Let  $\{\mathbb{P}_t\}_{t \geq 1}$  be a sequence of distributions and let  $\mathbb{P}_0$  be a target distribution such that for some  $q > 0$ ,*

$$d(\mathbb{P}_t, \mathbb{P}_0) \lesssim t^{-q}.$$

Define the Cesàro averages

$$\bar{\mathbb{P}}_t := \frac{1}{t} \sum_{j=1}^t \mathbb{P}_j.$$

Then

$$d(\bar{\mathbb{P}}_t, \mathbb{P}_0) \lesssim t^{-\min\{q, 1\}},$$

up to a  $\log t$  factor in the boundary case  $q = 1$ .

*Proof.* By convexity of  $d$  in its second argument,

$$d(\bar{\mathbb{P}}_t, \mathbb{P}_0) = d\left(\mathbb{P}_0, \frac{1}{t} \sum_{j=1}^t \mathbb{P}_j\right) \leq \frac{1}{t} \sum_{j=1}^t d(\mathbb{P}_0, \mathbb{P}_j) \lesssim \frac{1}{t} \sum_{j=1}^t j^{-q}.$$

Standard  $p$ -series asymptotics yield

$$\frac{1}{t} \sum_{j=1}^t j^{-q} \asymp \begin{cases} t^{-q}, & 0 < q < 1, \\ t^{-1} \log t, & q = 1, \\ t^{-1}, & q > 1, \end{cases}$$

which is  $t^{-\min\{q, 1\}}$  up to a logarithmic factor for  $q = 1$ .  $\square$

## Proof of Theorem 4.3

*Proof.* At step  $t$ , write the real-data average

$$\bar{\mathbb{P}}_t^{\text{bias}} := \frac{1}{t} \sum_{j=1}^t \mathbb{P}_j^{\text{bias}}.$$

Then

$$\mathbb{Q}_t = \frac{tm_1}{M_t} \bar{\mathbb{P}}_t^{\text{bias}} + \frac{m_2}{M_t} \sum_{j=1}^{t-1} \hat{\mathbb{P}}_j.$$

Using the triangle inequality,

$$d(\hat{\mathbb{P}}_t, \mathbb{P}_0) \leq d(\hat{\mathbb{P}}_t, \mathbb{Q}_t) + d(\mathbb{Q}_t, \mathbb{P}_0).$$

**Step 1: Learning error and bias term.** By Assumption A1,

$$d(\widehat{\mathbb{P}}_t, \mathbb{Q}_t) \lesssim M_t^{-p}.$$

For the bias term, convexity of  $d$  in its second argument gives

$$\begin{aligned} d(\mathbb{Q}_t, \mathbb{P}_0) &= d\left(\mathbb{P}_0, \frac{tm_1}{M_t} \bar{\mathbb{P}}_t^{\text{bias}} + \frac{m_2}{M_t} \sum_{j=1}^{t-1} \widehat{\mathbb{P}}_j\right) \\ &\leq \frac{tm_1}{M_t} d(\mathbb{P}_0, \bar{\mathbb{P}}_t^{\text{bias}}) + \frac{m_2}{M_t} \sum_{j=1}^{t-1} d(\mathbb{P}_0, \widehat{\mathbb{P}}_j). \end{aligned}$$

By Theorem B.1,

$$d(\bar{\mathbb{P}}_t^{\text{bias}}, \mathbb{P}_0) \lesssim t^{-\min\{q,1\}} \quad (\text{up to } \log t \text{ if } q = 1).$$

Since  $M_t \asymp t(m_1 + m_2)$ ,

$$\frac{tm_1}{M_t} d(\bar{\mathbb{P}}_t^{\text{bias}}, \mathbb{P}_0) \lesssim t^{-\min\{q,1\}}.$$

Define

$$d_t := d(\widehat{\mathbb{P}}_t, \mathbb{P}_0), \quad S_{t-1} := \sum_{j=1}^{t-1} d_j.$$

We obtain the basic recursion

$$d_t \lesssim M_t^{-p} + t^{-\min\{q,1\}} + \frac{m_2}{M_t} S_{t-1}. \quad (6)$$

**Step 2: Recursion for the partial sums.** Repeating the argument at step  $t-1$  gives

$$d_{t-1} \lesssim M_{t-1}^{-p} + (t-1)^{-\min\{q,1\}} + \frac{m_2}{M_{t-1}} S_{t-2}.$$

Hence

$$S_{t-1} = d_{t-1} + S_{t-2} \lesssim M_{t-1}^{-p} + (t-1)^{-\min\{q,1\}} + \left(1 + \frac{m_2}{M_{t-1}}\right) S_{t-2}.$$

Iterating yields

$$S_{t-1} \lesssim \sum_{j=1}^{t-1} \left( M_j^{-p} + j^{-\min\{q,1\}} \right) \left[ \prod_{k=j}^{t-2} \left( 1 + \frac{m_2}{M_k} \right) \right]. \quad (7)$$

**Step 3: Substituting back.** Substituting (7) into (6) gives

$$\begin{aligned} d_t &\lesssim M_t^{-p} + t^{-\min\{q,1\}} + \frac{m_2}{M_t} \sum_{j=1}^{t-2} \left( M_j^{-p} + j^{-\min\{q,1\}} \right) \left[ \prod_{k=j}^{t-2} \left( 1 + \frac{m_2}{M_k} \right) \right] \\ &\lesssim M_t^{-p} + t^{-\min\{q,1\}} + (1-\alpha) \sum_{j=1}^{t-2} \left( M_j^{-p} + j^{-\min\{q,1\}} \right) \left[ \frac{1}{M_t} \prod_{k=j}^{t-2} \left( 1 + \frac{m_2}{M_k} \right) \right]. \end{aligned}$$

Using  $M_t \asymp t(m_1 + m_2)$  and

$$\alpha = \frac{m_1}{m_1 + m_2}, \quad \frac{m_2}{M_t} \asymp \frac{1 - \alpha}{t},$$

the remainder of the proof proceeds exactly as in the unbiased case:

$$\frac{1}{t} \prod_{k=j}^{t-2} \left(1 + \frac{1 - \alpha}{k}\right) \asymp t^{-\alpha} j^{-(1-\alpha)}.$$

In this form, the three effects are additive:

$$\begin{aligned} d_t &\lesssim M_t^{-p} + t^{-\min\{q,1\}} + (1 - \alpha) t^{-\alpha} \sum_{j=1}^{t-2} (M_j^{-p} + j^{-\min\{q,1\}}) j^{-(1-\alpha)} \\ &\lesssim t^{-p} + t^{-\min\{q,1\}} + t^{-\alpha} \sum_{j=1}^{t-2} (j^{-1-(p-\alpha)} + j^{-1-(\min\{q,1\}-\alpha)}) \\ &\lesssim t^{-p} + t^{-\min\{q,1\}} + \begin{cases} t^{-\alpha}, & p > \alpha, \\ t^{-\alpha} \log t, & p = \alpha, \\ t^{\alpha-p}, & p < \alpha, \end{cases} + \begin{cases} t^{-\alpha}, & \min\{q, 1\} > \alpha, \\ t^{-\alpha} \log t, & \min\{q, 1\} = \alpha, \\ t^{-\min\{q,1\}}, & \min\{q, 1\} < \alpha, \end{cases} \\ &\lesssim t^{-p} + t^{-\min\{q,1\}} + t^{-\min\{p,\alpha\}} + t^{-\min\{q,1\}} \\ &\lesssim t^{-\min\{p,q,\alpha\}}, \end{aligned}$$

up to a log factor. We again observe that all asymptotic inequalities may be replaced by their equivalents in probability.  $\square$

## C Additional Experimental Details

This appendix provides a detailed description of the simulation pipeline for all simulations, including the underlying data-generating process, numerical grids, estimators, metrics, and the recursive procedure used to combine real and synthetic data.

### C.1 CRT Simulations - ECDF and KDE

In the CRT simulations of Section 5, the target distribution  $\mathbb{P}_0$  is a 1-dimensional mixture of two Gaussian components. This smooth distribution serves as the ground truth throughout both experiments. A numerical grid covering the effective support of  $\mathbb{P}_0$  is constructed once and used for all deterministic evaluations of distributional discrepancies. The true density and CDF of  $\mathbb{P}_0$  are available in closed form on this grid.

Both simulations follow the CRT procedure in Definition 3.3. At iteration  $t$ , a batch of  $m_1$  real samples drawn from  $\mathbb{P}_0$  is added to the accumulated dataset, along with  $m_2 = ((1 - \alpha)/\alpha)m_1$  synthetic samples drawn from the current generator  $\widehat{\mathbb{P}}_{t-1}$ .

In the CRT simulations, we use two estimators: the empirical distribution of the accumulated sample as the estimator  $\widehat{\mathbb{P}}_t$ , and a kernel density estimator whose bandwidth is chosen to correspond to a baseline smoothness parameter  $p$ ; the KDE thus serves as a concrete model with known uncontaminated convergence rate. In both settings, the estimator at iteration  $t$  defines a density and distribution function  $(\widehat{f}_t, \widehat{F}_t)$  evaluated on the numerical grid.

The primary metric is the  $W_1$  distance,

$$W_1(\widehat{\mathbb{P}}_t, \mathbb{P}_0) \approx \int |F_0(x) - \widehat{F}_t(x)| dx,$$

computed using the trapezoidal rule on the fixed grid. The MMD is evaluated using the same plug-in approach applied to the grid-based density estimates.

To estimate convergence rates, we record the sequence of losses  $\{d(\widehat{\mathbb{P}}_t, \mathbb{P}_0)\}$  over iterations and fit a power law of the form

$$\log d(\widehat{\mathbb{P}}_t, \mathbb{P}_0) = a + b \log M_t.$$

After discarding an initial burn-in period, the fitted slope  $b$  yields the empirical rate. When  $\alpha = p$ , CRT theory predicts a logarithmic phase transition; in this case, losses are pre-normalized by  $\log t$  before regression. The resulting values of  $b$  are reported as the observed convergence rates under recursive contamination. Simulation parameter values are provided below:

| Parameter              | Value                      | Description                              |
|------------------------|----------------------------|--|
| $m_1$                  | 50                         | Real samples per iteration               |
| $\alpha$               | $\{0.0, 0.1, \dots, 0.9\}$ | Real-data fraction                       |
| $T$                    | 2000                       | Total CRT iterations                     |
| $n_{\text{reps}}$      | 100                        | Number of repetitions                    |
| $m_{\text{grid}}$      | 200                        | Grid size for deterministic evaluation   |
| $[x_{\min}, x_{\max}]$ | Mixture-based              | Grid interval for density/CDF evaluation |
| $w_1$                  | 0.35                       | Mixture weight                           |
| $\mu_1, \sigma_1$      | -2.0, 0.8                  | First Gaussian component                 |
| $\mu_2, \sigma_2$      | 1.0, 1.3                   | Second Gaussian component                |
| $h_0$                  | 0.5                        | Base KDE bandwidth                       |

Table 3: CRT Simulation parameters for KDE and ECDF estimators.

Finally, we also show the estimated densities in each case, for every  $\alpha$  in Figure 7 and Figure 8.

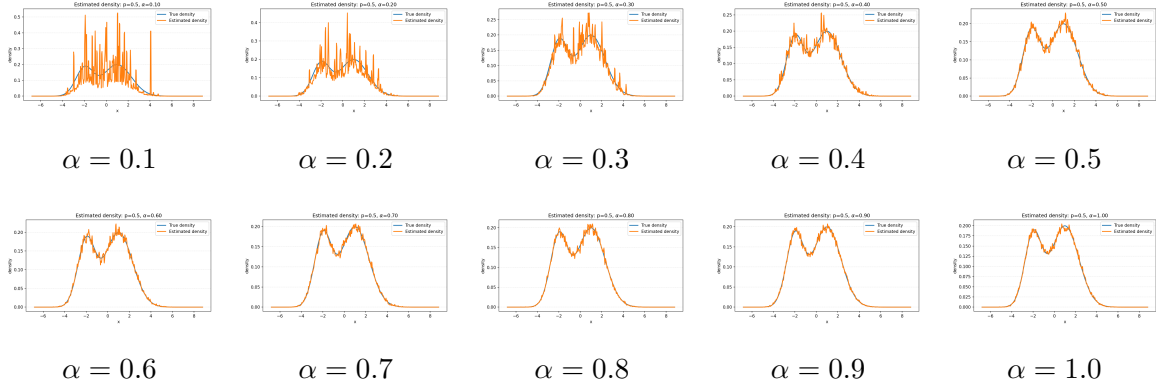


Figure 7: CRT Simulation (ECDF Estimator). Final output distributions  $\hat{\mathbb{P}}_T$  for varying values of  $\alpha$  (real data fraction) where all models are run for the same number of CRT iterations. This fixed compute budget for all models was chosen to minimize the effect of numerical plateaus in the loss when computing optimal transport distances after models have fully converged. Under this fixed compute budget, models at greater  $\alpha$  are shown to converge more easily, however, all for all  $\alpha$  we observe the predicted rate of convergence.

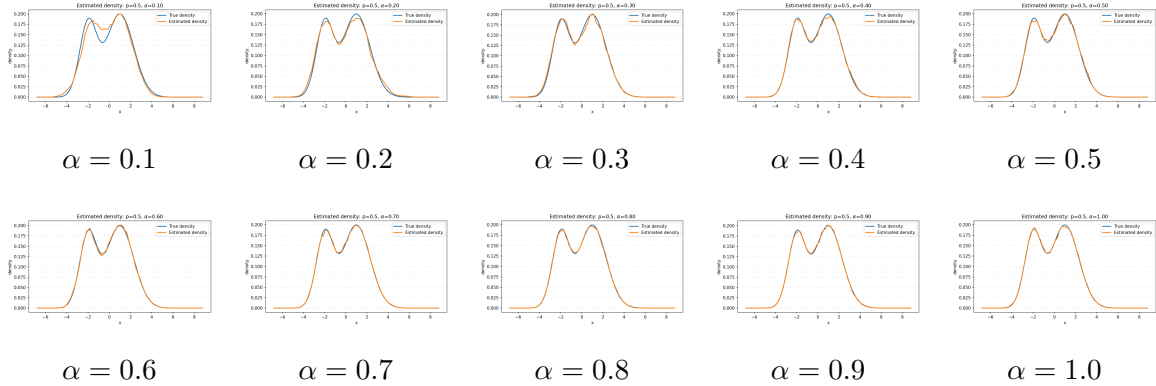


Figure 8: CRT Simulation (KDE Estimator). Final output distributions  $\hat{\mathbb{P}}_T$  for varying values of  $\alpha$  (real data fraction) where all models are run for the same number of CRT iterations. This fixed compute budget for all models was chosen to minimize the effect of numerical plateaus in the loss when computing optimal transport distances after models have fully converged. Under this fixed compute budget, models at greater  $\alpha$  are shown to converge more easily, however, all for all  $\alpha$  we observe the predicted rate of convergence.

## C.2 CRT Simulations - WGAN

In this simulation, the target distribution  $\mathbb{P}_0$  is the same as previous. The generator  $\widehat{\mathbb{P}}_t$  is implemented as a fully connected feedforward network. A latent vector  $z \in \text{Unif}(0, 1)$  is mapped through three 64 neuron hidden layers, LeakyReLU activations, and a final linear layer producing points in  $\mathbb{R}^1$ .

The iterations follow the CRT framework in Definition 3.3. At iteration  $t$ , a batch of  $m_1$  new samples from  $\mathbb{P}_0$  is appended to the dataset, together with  $m_2 = ((1 - \alpha)/\alpha)m_1$  synthetic samples generated from the previous iterate  $\widehat{\mathbb{P}}_{t-1}$ . At each CRT iteration, the generator is completely re-initialized, and is then trained for  $k$  epochs using minibatch stochastic gradient descent on the current accumulated dataset of real and synthetic samples. Optimization uses Adam with a fixed learning rate and weight decay.

The training loss is a differentiable optimal-transport discrepancy. Here, we employ an empirical  $W_1$  loss computed via quantile (inverse CDF) matching from the Python OT package (Flamary et al., 2021). At each iteration, convergence is assessed by computing an empirical Wasserstein-1 distance between  $\widehat{\mathbb{P}}_t$  and  $\mathbb{P}_0$ , using fresh evaluation batches of synthetic samples against a fixed large sample of the target distribution. This produces a sequence  $W_1(\widehat{\mathbb{P}}_t, \mathbb{P}_0)$  indexed by the effective sample size  $M_t$ .

To estimate convergence rates, we fit a power law of the form

$$\log W_1(\widehat{\mathbb{P}}_t, \mathbb{P}_0) = a + b \log M_t,$$

after discarding an initial burn-in period. When  $\alpha = p$ , CRT theory predicts a logarithmic phase transition; in this regime, the losses are normalized by  $\log(t)$  prior to regression. The fitted slope  $b$  is reported as the observed convergence rate of the recursive neural estimator. The results are shown in Figure 9, 10, 11.

| Parameter           | Value                      | Description  |
|---------------------|----------------------------|--|
| $m_1 + m_2$         | 500                        | Total samples per iteration                              |
| $\alpha$            | $\{0.1, 0.2, \dots, 1.0\}$ | Real-data fraction                                       |
| $T$                 | 500                        | Total CRT (outer training loop) iterations               |
| $k$                 | 25                         | Training epochs per CRT iteration (inner training loop)  |
| Latent dimension    | 1                          | Dimension of $z$   |
| Latent distribution | Uniform(0,1)               | Input to generator                                       |
| Network width       | 64                         | Hidden layer width                                       |
| Network layers      | 3                          | Number of hidden layers                                  |
| Activation          | LeakyReLU(0.02)            | Nonlinearity   |
| Optimizer           | Adam                       | Generator optimization                                   |
| Learning rate       | $2 \times 10^{-4}$         | Step size  |
| Weight decay        | $1 \times 10^{-3}$         | Optimizer weight decay                                   |
| Batch size          | 1024                       | Training minibatch size                                  |
| Loss type           | Quantile $W_1$             | Empirical Wasserstein-1 loss using POT package           |
| Evaluation Samples  | 200000                     | Number of samples (real, synthetic) for evaluation $W_1$ |

Table 4: CRT Simulation parameters for WGAN estimator.

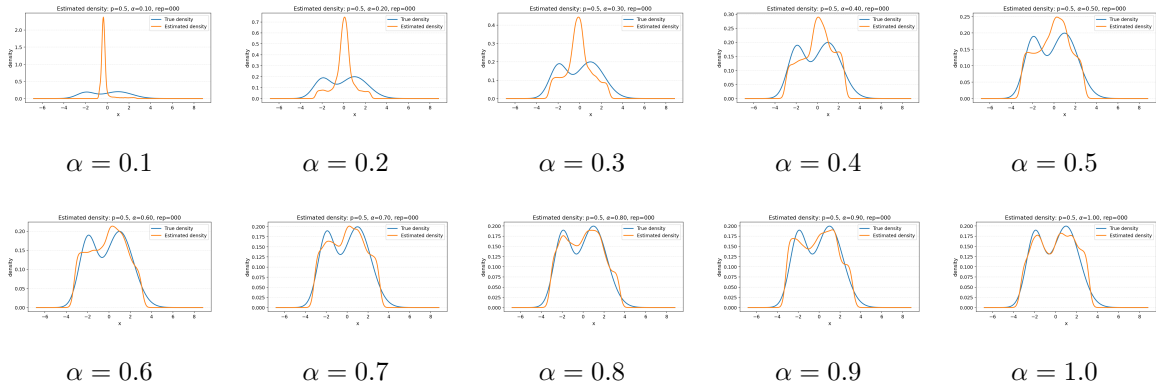


Figure 9: CRT Simulation (WGAN Estimator). Final output distributions  $\hat{\mathbb{P}}_T$  for varying values of  $\alpha$  (real data fraction) visualized via KDE, where all models are run for the same number of CRT iterations. This fixed compute budget for all models was chosen to minimize the effect of numerical plateaus in the loss when computing optimal transport distances after models have fully converged. Under this fixed compute budget, models at greater  $\alpha$  are shown to converge more easily, however, all for all  $\alpha$  we observe the predicted rate of convergence.

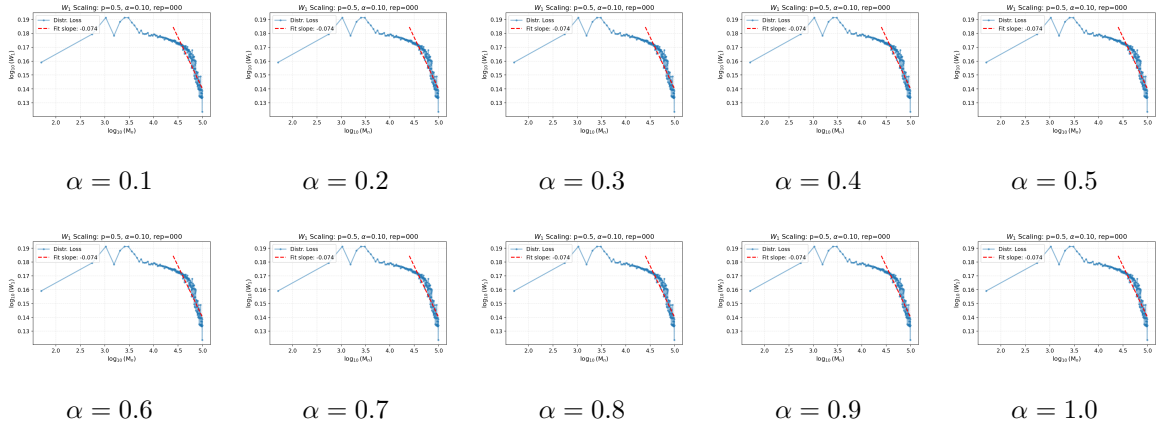


Figure 10: CRT Simulation (WGAN Estimator). Final  $W_1$  distributional losses and fitted slopes  $\alpha$  (real data fraction) for a single run.

### C.3 BCRT Simulations

In the BCRT setting, we use the same one-dimensional Gaussian mixture target distribution  $\mathbb{P}_0$  as in the CRT simulations, with identical mixture weights and component parameters. The numerical grid used to evaluate distributional discrepancies, as well as the closed-form density and CDF of  $\mathbb{P}_0$  on this grid, are constructed exactly as described in the previous

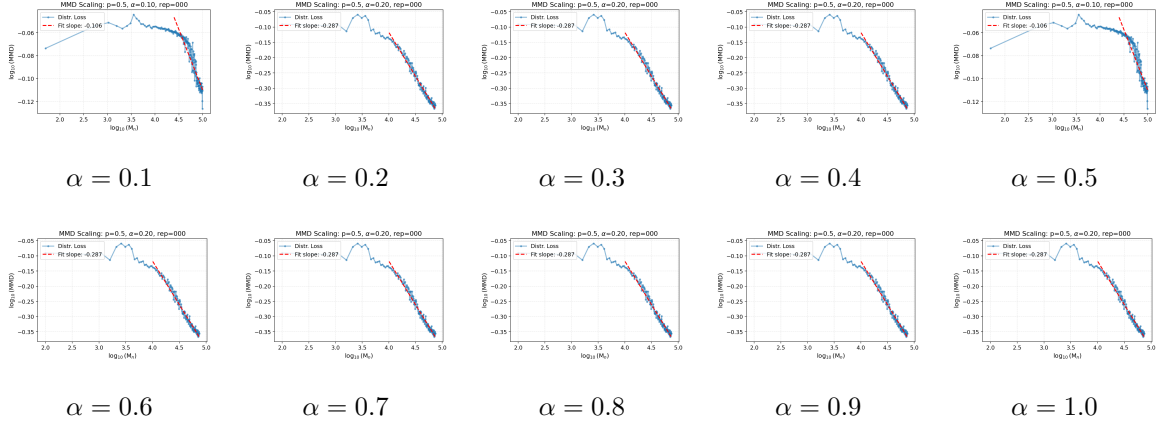


Figure 11: CRT Simulation (WGAN Estimator). Final MMD distributional losses and fitted slopes  $\alpha$  (real data fraction) for a single run.

subsection and reused throughout.

Here, we follow the BCRT procedure of Definition 4.1. At iteration  $t$ , a batch of  $m_1$  real samples is added to the accumulated dataset, together with  $m_2 = ((1 - \alpha_{\text{real}})/\alpha_{\text{real}})m_1$  synthetic samples drawn from the current estimator  $\widehat{\mathbb{P}}_{t-1}$ . Synthetic samples are generated by resampling from the accumulated dataset and adding Gaussian noise with variance equal to the current KDE bandwidth. Unlike in the CRT simulations, the real data stream here is biased. Specifically, at iteration  $t$ , real samples are drawn from a contaminated distribution

$$\mathbb{P}_t^{\text{bias}} = (1 - \text{bias}_t)\mathbb{P}_0 + \text{bias}_t \mathcal{N}(\mu_3, \sigma_3),$$

where  $(\mu_3, \sigma_3) = (3.0, 1.0)$ . The contamination level decays polynomially as

$$\text{bias}_t = 0.2(t + 5)^{-q},$$

with decay rate parameter  $q > 0$ .

The estimator  $\widehat{\mathbb{P}}_t$  is a kernel density estimator, as in the CRT case. The bandwidth follows a deterministic decay schedule

$$h_t = h_0 t^{-p/2},$$

with baseline bandwidth  $h_0 = 2$  and smoothness parameter  $p = 0.5$ . The estimator defines a density-CDF pair  $(\widehat{f}_t, \widehat{F}_t)$  evaluated on the fixed grid, using trapezoidal integration and renormalization as in previous simulations.

Performance is evaluated using the same deterministic plug-in metrics as in Simulations 1 and 2: the Wasserstein-1 distance,

$$W_1(\widehat{\mathbb{P}}_t, \mathbb{P}_0) \approx \int |F_0(x) - \widehat{F}_t(x)| dx,$$

and squared maximum mean discrepancy (MMD), with the MMD computed using a Gaussian kernel on the evaluation grid.

To estimate convergence rates, we record the sequence of losses  $\{d(\hat{\mathbb{P}}_t, \mathbb{P}_0)\}$  over iterations and fit a power law of the form

$$\log d(\hat{\mathbb{P}}_t, \mathbb{P}_0) = a + b \log M_t,$$

where  $M_t$  denotes the total number of accumulated samples. After discarding an initial burn-in period, the fitted slope  $b$  yields the estimated empirical convergence rate. Theoretical predictions suggest that the effective rate is governed by  $\min(p, \alpha, q)$ ; empirical estimates are compared against this benchmark in the main text. Simulation parameters specific to this section are summarized below. Additionally, final fitted models are visualized in Figure 12 and 13.

| Parameter              | Value             | Description                              |
|------------------------|-------------------|--|
| $m_1$                  | 25                | Real samples per iteration               |
| $\alpha$               | {0.25, 0.5, 0.75} | Real-data fraction                       |
| $q$                    | {0.25, 0.5, 0.75} | Bias Convergence Rate                    |
| $T$                    | 2000              | Total BCRT iterations                    |
| $n_{\text{reps}}$      | 100               | Number of repetitions                    |
| $m_{\text{grid}}$      | 200               | Grid size for deterministic evaluation   |
| $[x_{\min}, x_{\max}]$ | Mixture-based     | Grid interval for density/CDF evaluation |
| $w_1$                  | 0.35              | Mixture weight                           |
| $\mu_1, \sigma_1$      | -2.0, 0.8         | First Gaussian component                 |
| $\mu_2, \sigma_2$      | 1.0, 1.3          | Second Gaussian component                |
| $\mu_3, \sigma_3$      | 3.0, 1.0          | Bias Gaussian component                  |
| $h_0$                  | 2.0               | Base KDE bandwidth                       |

Table 5: BCRT Simulation (ECDF Estimator) experimental parameters.

| Parameter              | Value             | Description                              |
|------------------------|-------------------|--|
| $m_1$                  | 50                | Real samples per iteration               |
| $\alpha$               | {0.25, 0.5, 0.75} | Real-data fraction                       |
| $q$                    | {0.25, 0.5, 0.75} | Bias Convergence Rate                    |
| $T$                    | 2000              | Total BCRT iterations                    |
| $n_{\text{reps}}$      | 20                | Number of repetitions                    |
| $m_{\text{grid}}$      | 200               | Grid size for deterministic evaluation   |
| $[x_{\min}, x_{\max}]$ | Mixture-based     | Grid interval for density/CDF evaluation |
| $w_1$                  | 0.35              | Mixture weight                           |
| $\mu_1, \sigma_1$      | -2.0, 0.8         | First Gaussian component                 |
| $\mu_2, \sigma_2$      | 1.0, 1.3          | Second Gaussian component                |
| $\mu_3, \sigma_3$      | 3.0, 1.0          | Bias Gaussian component                  |
| $h_0$                  | 2.0               | Base KDE bandwidth                       |

Table 6: BCRT Simulation (KDE Estimator) experimental parameters

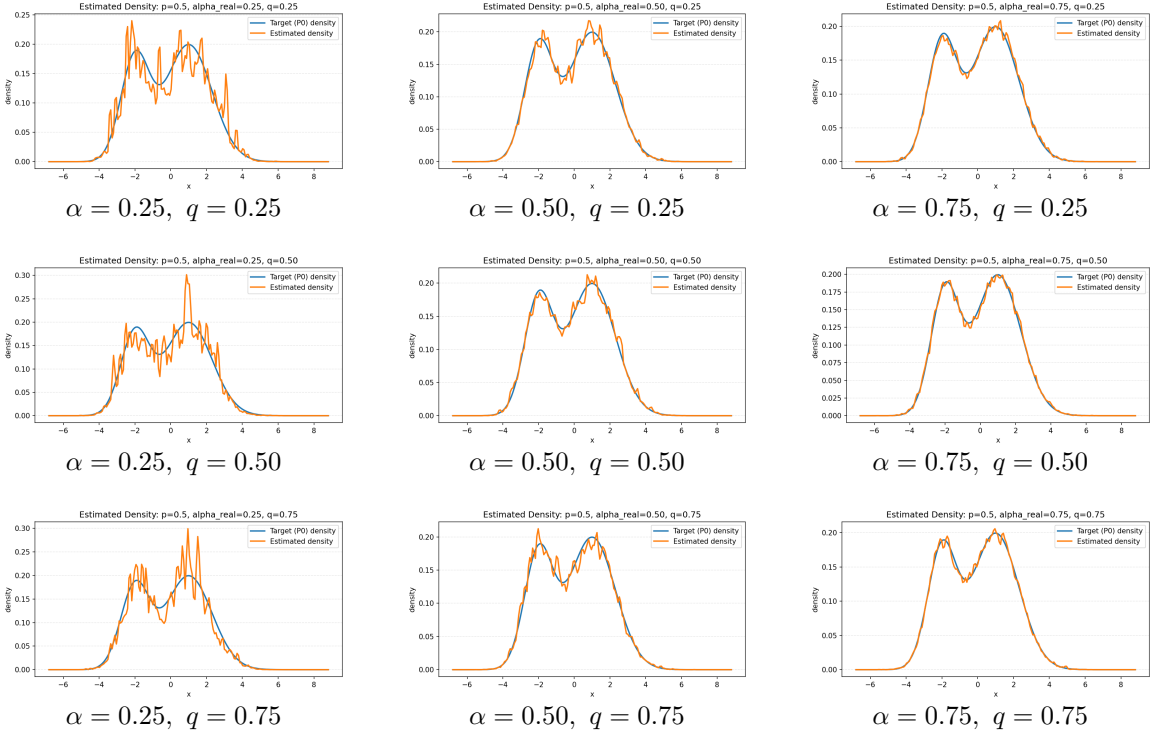


Figure 12: BCRT Simulation (ECDF Estimator). Final output distributions across combinations of real data fraction  $\alpha \in \{0.25, 0.5, 0.75\}$  and quantile level  $q \in \{0.25, 0.5, 0.75\}$ .

#### C.4 MNIST

Here we present experimental parameters of the DDPM diffusion model trained on MNIST under CRT. We use data from the 60,000 MNIST training set where each training sample is used by the optimizer an equal number of epochs, as per the setup in Theorem 3.4. More specifically, each iteration builds on the previous model’s generator, such that every new sample is trained for a fixed number of epochs and all datapoints are used by the optimizer for equal number of training steps. A new sample is drawn at each CRT iteration to visualize the output of each iteration’s generator.

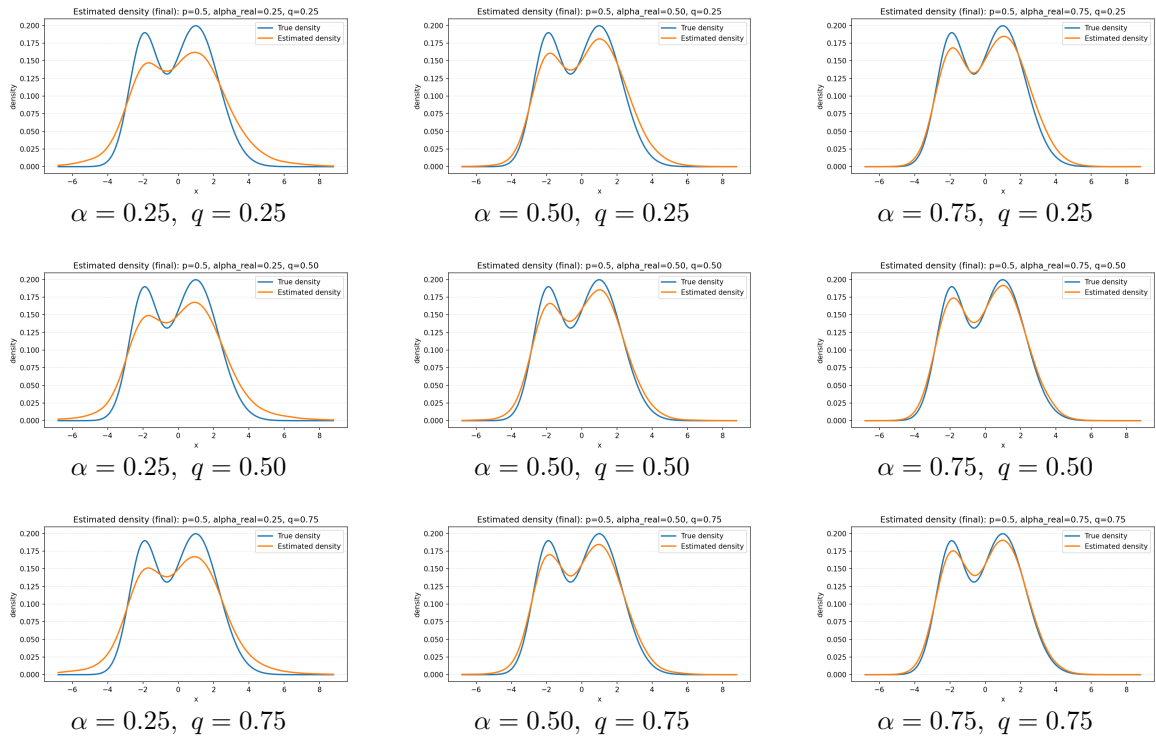


Figure 13: BCRT Simulation (KDE Estimator). Final output distributions across combinations of real data fraction  $\alpha \in \{0.25, 0.5, 0.75\}$  and bias rate  $q \in \{0.25, 0.5, 0.75\}$ .

Table 7: Experimental parameters for MNIST experiment.

| Parameter       | Value                       | Description                                  |
|-----------------|-----------------------------|--|
| $\alpha$        | $\{0.25, 0.5, 0.75, 1.00\}$ | Real-data fraction                           |
| $m_1$           | 200                         | Real samples per iteration                   |
| $T$             | 300                         | Total CRT iterations                         |
| $T_{diff}$      | 200                         | Number of diffusion steps                    |
| Epochs          | 150                         | Epochs of training per data iteration        |
| Schedule        | Cosine                      | Optimizer schedule                           |
| $\beta_{start}$ | $1 \times 10^{-4}$          | Noise variance schedule                      |
| $\beta_{end}$   | $2 \times 10^{-2}$          | Noise variance schedule                      |
| Time dimension  | 128                         | Dimension of embedding for time conditioning |

Finally we present the details of the network architecture. We parameterize the diffusion noise predictor using a lightweight UNet-style convolutional network with residual blocks and time conditioning. The timestep  $t$  is embedded via a sinusoidal encoding and passed through a small MLP.

Architectually, the model follows a two-level UNet structure, where the encoder consists

of an initial convolution followed by residual blocks and two stages of downsampling from 28x28 to 7x7 while increasing channel width from 64 to 128. The bottleneck consists of residual blocks while the decoder mirrors the encoder with two stages of upsampling and skip connections. The final convolution maps features back to the single output channel predicting the noise.